

# MILKY WAY DARK MATTER DISTRIBUTION OR MOND TEST FROM VERTICAL STELLAR KINEMATICS WITH GAIA DR3

MARTÍN LÓPEZ-CORREDOIRA<sup>1,2,3</sup>  
*Draft version December 16, 2024*

## ABSTRACT

Vertical stellar kinematics+density can be used to trace the dark matter distribution [or the equivalent phantom mass in a Modified Newtonian Dynamics (MOND) scenario] through Jeans equations. In this paper, we want to improve this type of analysis by making use of the recent data of the 6D information from the Gaia-DR3 survey in the anticenter and the Galactic poles to obtain the dynamical mass distribution near plane regions, including extended kinematics over a wide region of  $8 \text{ kpc} < R < 22 \text{ kpc}$ ,  $|z| < 3 \text{ kpc}$ .

Our conclusions are as follows: (i) the model of the spherical dark matter halos and the MOND model are compatible with the data; (ii) the model of the disk dark matter (with density proportional to the gas density) is excluded; (iii) the total lack of dark matter (there is only visible matter) within Newtonian gravity is compatible with the data; for instance, at solar Galactocentric radius, we obtained  $\Sigma = 39 \pm 18 \text{ M}_\odot \text{ pc}^{-2}$  for  $z = 1.05 \text{ kpc}$ , compatible with the expected value for visible matter alone of  $44 \text{ M}_\odot \text{ pc}^{-2}$ , thus allowing zero dark matter. Similarly, for  $R > R_\odot$ ,  $z = 1.05 \text{ kpc}$ :  $\Sigma = 28.7 \pm 9.6$ ,  $23.0 \pm 5.7$ ,  $16.9 \pm 5.8$ ,  $11.4 \pm 6.6 \text{ M}_\odot \text{ pc}^{-2}$ , respectively, for  $R = 10, 13, 16, 19 \text{ kpc}$ , compatible with visible matter alone. Larger error bars in comparison with previous works are not due to worse data or a more awkward technique but to a stricter modeling of the stellar distribution.

*Keywords:* Stellar kinematics (1608) — Galaxy dynamics (591) — Dark matter (353) — Milky Way disk (1050).

## 1. INTRODUCTION

The hypothesis of the existence of dark matter halos in galaxies like the Milky have different motivations, either from cosmology, extragalactic astronomy, or investigations in our own Galaxy (e.g., López-Corredoira 2022, §3.3).

One of the first observational evidence for the missing mass in our Galaxy was provided by the fact that the Galactic mass derived from the motions of distant globular clusters was approximately three times larger than that obtained from the rotation of the inner disk of the Galaxy (Finzi 1963). Over many decades, the rotation curve of the Galactic disk in the gas component (e.g., Clemens 1985; Brand & Blitz 1993) or the stellar component (e.g., Pont et al. 1997; Battinelli et al. 2013) or masers (e.g., Honma et al. 2012; Reid et al. 2014) has also been investigated, or the motion of satellite galaxies orbiting the Milky Way (e.g., Sofue 2015; Callingham et al. 2019). However, velocities in galaxy pairs and satellites might also measure the mass of the intergalactic medium filling the space between the members of the pairs rather than the mass of dark halos supposedly associated with the galaxies (López-Corredoira et al. 1999;

López-Corredoira et al. 2002a).

In spite of the large number of studies, the consensus knowledge of the characteristics of the dark matter halo derived from rotation curves is still small. First, there is a huge dispersion of the values of the total mass of the Galaxy, including this halo, with values as small as  $3 - 4 \times 10^{11} \text{ M}_\odot$  (Sofue 2009; Ou et al. 2024), or as large as  $2.2 \times 10^{12} \text{ M}_\odot$  (Sakamoto et al. 2003). Second, there is not even consensus on whether the rotation curve is flat (Olling & Merrifield 2000; Sofue et al. 2009) or Keplerian (Honma & Sofue 1996; Galazutdinov et al. 2015; Jiao et al. 2023) over some Galactocentric distance in the outer disk or something in between with a slight decline (Koop et al. 2024).

Rotation curves in spiral galaxies can also be explained with hypotheses different from the standard dark matter halos of non-baryonic cold dark matter (López-Corredoira 2022, Section 3.6): with different types of dark matter, even baryonic, magnetic fields, non-circular orbits in the outer disk, alternative gravity theories. The most popular alternative to dark matter is the modification of gravity laws proposed in Modified Newtonian Dynamics (MOND; Sanders & McGaugh (2002); Famaey & McGaugh (2012)), which modifies the Newtonian law for accelerations lower than a constant  $a_0$ , or dark matter distributed in the outer disk instead of a halo (Bosma 1981; Pfenninger et al. 1994; Feng & Gallo 2015; McKee et al. 2015; Fernández-Torija 2016; Kramer & Randall 2016; Sipols & Pavlovich 2021; Sylos Labini et al. 2023; 2024; Sylos Labini 2024) (disk dark matter). Here, we

<sup>1</sup> Instituto de Astrofísica de Canarias, E-38205 La Laguna, Tenerife, Spain; martin@lopez-corredoira.com

<sup>2</sup> PIFI-Visiting Scientist 2023 of Chinese Academy of Sciences at Purple Mountain Observatory, Nanjing 210023, and National Astronomical Observatories, Beijing 100012

<sup>3</sup> Departamento de Astrofísica, Universidad de La Laguna, E-38206 La Laguna, Tenerife, Spain

will focus on MOND and disk dark matter apart from the standard (spheroidal or slightly ellipsoidal) halo dark matter.

Apart from rotation curves, there are other ways to quantify or trace the putative dark matter distribution, although can indeed be solved without dark matter: galactic stability (Toomre 1981) or warp creation (López-Corredoira et al. 2002a), for instance.

Kinematics of stars can be used in a different way to trace the dark matter distribution (or the equivalent phantom mass in a MOND scenario), particularly using the vertical velocities of stars rather than the rotation speed. Moni Bidin et al. (2012b) used Jeans equations to relate dispersion of vertical stellar velocities, stellar density distribution, and dark matter density. The dynamical surface mass density at the solar position with a distance to the Galactic plane between  $z = 1.5$  and  $4$  kpc was estimated using the velocity dispersion of thick disk stars (Moni Bidin et al. 2012a), resulting in compatibility with the expectations of visible mass alone. No dark component was required to account for the observations, all the current models of a spherical dark matter halo were excluded at a confidence level higher than  $4\sigma$ . This result has been criticized on several grounds (e.g., Sanders 2012; Bovy & Tremaine 2012), such as the calculation of the velocity dispersion or the assumptions in the calculations. The criticisms have been responded to (Moni Bidin et al. 2015). Indeed, the general impression among many different authors is that the measured mass density is highly dependent on the assumptions using the Jeans equations (e.g., Candlish et al. 2016; Cheng et al. 2024). In particular, the consideration of the disk as a double component of thin+thick disks, the vertical profile of stellar density (exponential or  $\text{sech}^2$ ), the flare, and other considerations matter (Sánchez-Salcedo et al. 2016; Nitschai et al. 2021).

In this paper, we want to improve upon this type of analysis by revising the equation, taking into account subtle details of the distribution in Section 2, making use of the recent data on the 6D information from the Gaia-DR3 survey (Gaia Collaboration 2023), including extended kinematics over a wide region up to  $R > 20$  kpc by means of a deconvolution technique of the parallax errors in Section 3. We will also use accurate information on the stellar and gas+dust density distribution, considering their error bars. All of this will serve to derive the dark (total - visible) matter distribution in the range  $8 < R(\text{kpc}) < 22$ ,  $|z| < 3$  kpc, which may distinguish between spheroidal halo dark matter and disk dark matter in Section 4. We also carry out the full analysis under the considerations of a MOND scenario in Section 5. Systematic errors are considered in Section 6. A discussion is given in Section 7.

## 2. DENSITY DERIVED FROM STELLAR KINEMATICS

Given an axisymmetric mass distribution  $\rho(R, z)$ , the surface density within a finite distance  $z$  of the plane is defined as

$$\Sigma(R, z) \equiv \int_{-z}^z \rho(R, z') dz'. \quad (1)$$

Using Poisson equation, we get

$$4\pi G \Sigma(R, z) = \frac{1}{R} \int_{-z}^z \frac{\partial [R a_R(R, z')]}{\partial R} dz' \quad (2)$$

$$+ [a_z(R, z) - a_z(R, -z)],$$

where  $a_R$  (related to the rotation curve as  $V_c^2 = R a_R$ ) and  $a_z$  are the accelerations due to the given potential and, assuming steady equilibrium, can be related through the Jeans equations with the kinematics of the stellar distribution with density of  $\rho_*(R, z)$  (Moni Bidin et al. 2012b; Loebman et al. 2012; Villa Durango 2022):

$$V_c^2(R, z) = R a_R(R, z) = - \frac{R}{\rho_*(R, z)} \frac{\partial [\rho_*(R, z) \overline{V_R^2}(R, z)]}{\partial R} \quad (3)$$

$$- \frac{R}{\rho_*(R, z)} \frac{\partial [\rho_*(R, z) \overline{V_R V_Z}(R, z)]}{\partial z} - \overline{V_R^2}(R, z) + \overline{V_\phi^2}(R, z),$$

$$a_z(R, z) = - \frac{\overline{V_R V_Z}(R, z)}{R} - \frac{1}{\rho_*(R, z)} \frac{\partial [\rho_*(R, z) \overline{V_R V_Z}(R, z)]}{\partial R} \quad (4)$$

$$- \frac{1}{\rho_*(R, z)} \frac{\partial [\rho_*(R, z) \overline{V_z^2}(R, z)]}{\partial z}.$$

Note that in the Jeans equations, we use the stellar density  $\rho_*$  and not the total density  $\rho$  because our distribution function over which we measure the velocities is the stellar population alone; we have no information about the velocities of dark matter particles. This does not mean that we are neglecting the dark matter and gas here, but we separate the stellar component for our distribution function, embedded in a potential that includes everything (stars, gas, and dark matter). There is no problem of lack of self-consistency here. The Jeans equations describe the motion of any collection of particles in a gravitational field (e.g., Binney & Tremaine (2008, Section 4.8), Ciotti (2021, ch. 10), Moni Bidin et al. (2012b); Bovy & Tremaine (2012)). For a given gravitational field, each component of matter obeys a separate collisionless Boltzmann equation from which the Jeans equations are derived. In fact, even the distribution for any particular subtype of stars would obey a separate equation if we could measure the density and velocities of this subcomponent. In our case, we use a multicomponent with the density and velocity distribution average of all of the observed single subtypes of stars, where the Jeans equations keep the same dependence (see Appendix A).

The rotation curve is almost flat, with a very small decrease with  $R$  (Wang et al. 2023) ( $\beta$ ). We assume:

$$V_c(R, z)^2 = [V_c(R_\odot, z) + \beta(z)(R - R_\odot)]^2 \quad (5)$$

$$\approx V_c^2(R_\odot, z) + 2\beta(z)V_c(R_\odot, z)(R - R_\odot),$$

and  $V_z^2(R, z) = -V_z^2(R, -z)$ . Also, the terms with  $\overline{V_R V_Z}$  in Eq. (4) and its gradients can be neglected (Candlish et al. 2016; Eilers et al. 2019), because they are around two orders of magnitude smaller compared to the remaining terms (see also §3.4 including off-plane regions).

The stellar density is modeled with a thin+thick disk, with  $f$  the ratio of thick-to-total disk stars in the solar neighborhood, radial exponential dependence of scale length  $h_R$ , and vertical exponential or  $\text{sech}^2$  dependence with scale height  $h_z$  of each of the thin and thick subcomponents. There is plenty of literature discussing whether exponential or  $\text{sech}^2$  functions fit better the vertical distribution (e.g., Dobbie & Warren 2020; Everall et al.

2022; Chrobáková et al. 2022; Vieira et al. 2023), but in any case, both forms are almost equivalent at large  $|z|$ . The contribution of halo stars in the regions used,  $|z| < 3$  kpc, is negligible (Bilir et al. 2008). We include a flare (that is, variable scale heights instead of constant; for a more general expression of Jeans equations with flare, see also López-Corredoira et al. (2020, Eq. 13) or Nitschai et al. (2021)):

1. Vertical distribution as the sum of two exponentials:

$$\rho_*(R, z) = \rho_{*,\odot} \exp\left(-\frac{R - R_\odot}{h_R}\right) \quad (6)$$

$$\times \left[ (1 - f) \exp\left(-\frac{|z|}{h_{z,\text{thin}}(R)}\right) + f \exp\left(-\frac{|z|}{h_{z,\text{thick}}(R)}\right) \right],$$

2. or vertical distribution as the sum of two  $\text{sech}^2$  functions:

$$\rho_*(R, z) = \rho_{*,\odot} \exp\left(-\frac{R - R_\odot}{h_R}\right) \quad (7)$$

$$\times \left[ (1 - f) \text{sech}^2\left(\frac{|z|}{2h_{z,\text{thin}}(R)}\right) + f \text{sech}^2\left(\frac{|z|}{2h_{z,\text{thick}}(R)}\right) \right],$$

With all of these ingredients, we get

$$4\pi G\Sigma(R, z) \approx \frac{2V_c(R_\odot, z) \int_{-z}^z \beta(z') dz'}{R} - 2 \frac{\partial \overline{V_z^2}(R, z')}{\partial z} \quad (8)$$

$$+ \frac{2\overline{V_z^2}(R, z)}{\overline{h_z}(R, z)},$$

1. In a vertical distribution as the sum of two exponentials (Eq. 6)

$$\overline{h_z}(R, z) = \quad (9)$$

$$\left[ \frac{(1-f)}{h_{z,\text{thin}}(R)} + \frac{f}{h_{z,\text{thick}}(R)} \exp\left(|z| \frac{h_{z,\text{thick}}(R) - h_{z,\text{thin}}(R)}{h_{z,\text{thin}}(R)h_{z,\text{thick}}(R)}\right) \right]^{-1} \\ \left[ (1-f) + f \exp\left(|z| \frac{h_{z,\text{thick}}(R) - h_{z,\text{thin}}(R)}{h_{z,\text{thin}}(R)h_{z,\text{thick}}(R)}\right) \right]$$

2. In a vertical distribution as the sum of two  $\text{sech}^2$  functions (Eq. 7)

$$\overline{h_z}(R, z) =$$

$$\left[ \frac{(1-f)}{h_{z,\text{thin}}(R)} \tanh(x_{\text{thin}}) + \frac{f}{h_{z,\text{thick}}(R)} \frac{\text{sech}^2(x_{\text{thick}})}{\text{sech}^2(x_{\text{thin}})} \tanh(x_{\text{thick}}) \right]^{-1} \\ \left[ (1-f) + f \frac{\text{sech}^2(x_{\text{thick}})}{\text{sech}^2(x_{\text{thin}})} \right]$$

$$x_{\text{thin}} = \frac{|z|}{2h_{z,\text{thin}}(R)}; \quad x_{\text{thick}} = \frac{|z|}{2h_{z,\text{thick}}(R)} \quad (10)$$

Here,  $\overline{h_z}(R, z)$  stands for an equivalent average global scale height (or scale at which the variation of the density changes by factor  $e$  in the vertical direction), including thin and thick disks and their flares. The expression using the vertical distribution as a sum of two exponential has an inconsistency at  $z = 0$ , where we get  $\Sigma(z = 0) > 0$  if  $\overline{V_z^2}(R, z = 0) \neq 0$ , as it is the real case, whereas it

should be zero according to our own definition in Eq. (1). This derives from using a sum of exponential stellar distributions, which has  $\frac{1}{\rho_*} \frac{\partial \rho_*(z \rightarrow 0)}{\partial z} = \frac{1}{h_z}$  for each of the thin and thick components. However, if we assume in the limit of low  $z$  at  $\rho_* \propto \text{sech}^2(|z|/2h_z)$ , we get instead  $\frac{1}{\rho_*} \frac{\partial \rho_*(z \rightarrow 0)}{\partial z} = \frac{\tanh[|z|/(2h_z)]}{h_z} \approx \frac{|z|}{2h_z^2}$  for low  $|z|$ , converging to zero for the limit of  $z = 0$ . For this reason, we will adopt in the application throughout this paper the vertical distribution as the sum of two  $\text{sech}^2$  functions, although some application of the exponential profile will be carried out to check for consistency or differences. In any case, at intermediate-high  $z$ , both expressions are almost equivalent.

In practice, we can determine  $\overline{V_z^2}(R, z) = \overline{V_z^2}(R, z) + \sigma_{V_z}^2(R, z)$ . The average  $\overline{(\dots)}(R, z)$  includes bins with distance from the plane  $z$ . Both the average and dispersion of vertical velocities are provided from kinematic distribution of stars. Most authors (e.g., Moni Bidin et al. 2012b; Villa Durango 2022; Zhu et al. 2023) assume that  $\sigma_{V_z}$  falls exponentially with  $R$ , but this is not correct in a flared disk, and as a matter of fact, it is observed that  $\sigma_{V_z}$  has a minimum around  $R = 15$  kpc and it grows for larger  $R$  (Wang et al. 2023). We assume  $R_\odot = 8.34$  kpc throughout this paper.

### 3. ANALYSIS FROM EXTENDED KINEMATIC MAPS OF GAIA DR3

#### 3.1. Extended kinematic maps

We derive kinematic from the subsample of Gaia DR3, including radial velocities,<sup>4</sup> and carry out a deconvolution of parallax errors through an inversion technique based on Lucy's method (López-Corredoira & Sylos Labini 2019), allowing to reach much larger distances than with the direct determination of distance as the inverse of parallax for each star. The methodology and application to Gaia data have already been explained in previous works (López-Corredoira & Sylos Labini 2019; Wang et al. 2023). We have not included zero-point correction in the parallaxes of Gaia data. This has a negligible effect on the kinematic maps within the explored range of distances (López-Corredoira & Sylos Labini 2019; Wang et al. 2023).

Here, we repeat the analysis of Wang et al. (2023), adding a couple of improvements: (1) we remove the high-velocity stars ( $|V_R| > 100$  km/s,  $|V_z| > 100$  km/s,  $V_\phi < 0$ ,  $V_\phi > 400$  km/s), possibly related to the nonequilibrium state of the Galactic disk, and calculate the dispersion of velocities ( $\sigma_V$ ) taking into account this cut in the tail of the Gaussian distribution (see Appendix B); (2) we calculate  $\sigma_V$  directly from the dispersion of the velocity of stars once we know the average distance of each bin with a given parallax from Lucy's method, rather than an expansion as done in Wang et al. (2023).

<sup>5</sup> Our new calculation is more accurate, whereas Wang

<sup>4</sup> For a total of 32 million stars (Katz et al. 2023), Gaia RV targets were selected to include sources with  $G_{RVS} < 14$  covering the whole range of temperatures of the old population between F4 and M7 spectral types of any luminosity class.

<sup>5</sup> Wang et al. (2023)'s method:  $\sigma_{V_z} = \sqrt{\sin^2(b)[\sigma_{V_r}^2 - \Delta V_r^2] + \cos^2(b)r^2[\sigma_{\mu_b}^2 - \Delta \mu_b^2]}$ , where  $r$  is the heliocentric distance;  $\sigma_{V_r}$  and  $\Delta V_r$  are, respectively, the

et al. (2023)’s method gives slightly different results possibly due to non-negligible covariance terms. Our results for the median velocities,  $\bar{V}_z(R, z)$ , are in agreement with those obtained by Wang et al. (2023), and the  $\sigma_{V_z}$  are slightly lower, especially in off-plane regions because Wang et al. (2023) included few high-velocity stars that inflate  $\sigma_{V_z}$ , while the results here are more reliable.

Here, we only use data in two directions:

**Galactic poles:**  $|b| > 60^\circ$ ,  $\forall \ell$ ,  $R_\odot - 1 < R < R_\odot + 1$  kpc. This reaches the highest distance from the plane in Galactocentric radii close to the solar one.

**Anticenter:**  $160^\circ < \ell < 200^\circ$ ,  $\forall b$ . This allows it to reach a higher distance in the outer disk.

These lines of sight are little affected by extinction, so we can go farther in distance, and we are less affected by the uncertainties in the determination of average distance through the deconvolution technique.

### 3.2. Warp

The density distributions are not affected by the warp in these lines of sight of the anticenter because the amplitude of the warp is almost null in the azimuth corresponding to the anticenter (whereas the maximum absolute amplitude corresponds to azimuths around  $80^\circ$  and  $260^\circ$ ) (Chrobáková et al. 2022).

The average vertical velocity is slightly changed by the warp (López-Corredoira et al. 2020), but given the symmetry between northern and southern Galactic hemispheres, on average for both the positive and the negative Galactic latitudes, the effect of the warp within distances  $z$  from the plane is null. The dispersion of velocities, which is the relevant term used in the Jeans equations, is not affected by the warp.

Some researchers have speculated that the outer disk is in a nonstationary state due to some precession of the warp (e.g., Poggio et al. 2020). However, doubt has been cast upon the precession of the warp (Chrobáková & López-Corredoira 2021). In any case, even in the case of significant warp precession, it would affect few km/s (negligible) in the average vertical velocities toward the anticenter, and it does not affect the dispersion of velocities.

### 3.3. Scale height and flare of the thin and thick disks

Calculating the scale heights directly from the data of stars only with radial velocities has many uncertainties because this sample is incomplete, the luminosity function of the population is difficult to model, and there are some selection functions that need some corrections, which would make the calculation quite inaccurate. Instead, we will use the measurements of the scale heights for a complete sample with  $G < 19$  in Gaia data, which only needs the luminosity function to derive the distribution of all stars.

Chrobáková et al. (2022) derived the average scale height of the ‘whole population’ of Gaia EDR3/ $G < 19$ +Lucy’s deconvolution in the range of  $R$  between 5 and 20 kpc, assuming a ratio of thick disk stars in the

dispersion and error in radial velocities;  $\sigma_{\mu_b}$  and  $\Delta\mu_b$  are, respectively, the dispersion and error in proper motions in the direction perpendicular to the Galactic plane.

solar neighborhood of  $f = 0.09 \pm 0.01$ . With a second-order polynomial fit to the data of these scale heights and their errors in Chrobáková et al. (2022, Table 2), we get

$$h_{z,\text{thin},G<19}(R) = 0.14 - 0.0037R[\text{kpc}] + 0.0017R[\text{kpc}]^2 \text{ kpc} \quad (11)$$

$$h_{z,\text{thick},G<19}(R) = 1.21 - 0.19R[\text{kpc}] + 0.015R[\text{kpc}]^2 \text{ kpc},$$

$$\sigma_{h_z,\text{thin},<19} = 0.044 \text{ kpc}; \sigma_{h_z,\text{thick},<19} = 0.19 \text{ kpc};$$

$$E_{h_z,\text{thin},G<19} = |0.040 - 0.0080R[\text{kpc}] + 0.0005R[\text{kpc}]^2| \text{ kpc},$$

$$E_{h_z,\text{thick},G<19} = |0.63 - 0.14R[\text{kpc}] + 0.0072R[\text{kpc}]^2| \text{ kpc},$$

where  $E_{h_z,xxx}$  stands for the error in  $h_{z,xxx}$ . For the total error, we sum quadratically  $E$  and the  $\sigma$  of the fits of  $h_z$ . These numbers were derived assuming exponential distributions with  $z$ , but the scale heights in the solar neighborhood are very close to those obtained of Gaia stars with  $\text{sech}^2$  distributions (Vieira et al. 2023), and the flare parameters affect high  $z$  values where exponential and  $\text{sech}^2$  distributions are equivalent.

There may be some differences between the scale height derived for the  $G < 19$  Gaia sample and the stars with available radial velocity data (Gaia-RV targets; around 6-7% of the stars with  $G < 19$  in Gaia) data, i.e., those with brighter magnitudes. As said previously, Gaia-RV targets were selected to include sources with  $G < 14$  covering the whole range of temperatures of the old population between the F4 and M7 spectral types of any luminosity class (Katz et al. 2023). But this difference in scale heights between both samples is small because both of them trace a stellar population with approximately the same age.

Thick disk stars have a very narrow range of ages, so there is no significant difference in their average age in both surveys. Differences in the average age of the disk stars in our samples can be calculated with Besançon model (Robin et al. 2003; Amôres et al. 2017).<sup>6</sup> See Table 1 for Galactic pole and anticenter directions. We only test it in the anticenter direction for distances less than 6 kpc because the Besançon model has a disk cutoff beyond  $R = 14$  kpc. As can be observed, Gaia-RV targets have, on average, a lower age ( $t$ ) than the complete  $G < 19$  survey; on average, for the ten volumes in Table 1,  $\frac{\Delta t}{t} = -0.11$  with a dispersion of  $\sigma = 0.08$ ;  $\langle t \rangle \approx 6$  Gyr.

Scale height changes with age approximately as  $\frac{\Delta h_z}{h_z} \approx 0.6 \frac{\Delta t}{t}$  for  $t \approx 6$  Gyr (Rana & Basu 1992; MacKereth et al. 2017), so the scale height is on average 7% (with a dispersion of 5%) lower due to the change in average ages between the Gaia-RV targets and  $G < 19$  complete survey analyzed by Chrobáková et al. (2022), assuming Besançon model. This is not an accurate calculation, and it is model dependent. Moreover, the flare also depends on the stellar age (MacKereth et al. 2017), which we do not take here into account. Nonetheless, we may assume in a first-order approximation for this average variation of 7% of scale height in the thin disk with uncertainty of the dispersion for the different lines of sight; thus, our

<sup>6</sup> Simulations of the Besançon model of stellar population synthesis 1612 are available at <https://model.obs-besancon.fr/>

**Table 1**

Average age (in Gyr) of the thin disk stars, derived from Besançon model for different selection of sources according to the selected area centered at  $(\ell, b)$  with  $100 \text{ deg}^2$  and heliocentric distance ( $d$  in kpc); magnitude range in Gaia-G-band and spectral type.

|  | $G < 19$ | $G < 14/\text{F4-M7}$ |
|--|----------|-----------------------|
| $b = 90^\circ, 0 < d \leq 2$                   | 6.60     | 6.47                  |
| $\ell = 180^\circ, b = 5^\circ, 0 < d \leq 2$  | 4.91     | 4.32                  |
| $\ell = 180^\circ, b = 5^\circ, 2 < d \leq 4$  | 5.30     | 4.71                  |
| $\ell = 180^\circ, b = 5^\circ, 4 < d \leq 6$  | 5.35     | 3.79                  |
| $\ell = 180^\circ, b = 15^\circ, 0 < d \leq 2$ | 6.06     | 5.17                  |
| $\ell = 180^\circ, b = 15^\circ, 2 < d \leq 4$ | 6.95     | 6.70                  |
| $\ell = 180^\circ, b = 15^\circ, 4 < d \leq 6$ | 7.16     | 6.45                  |
| $\ell = 180^\circ, b = 25^\circ, 0 < d \leq 2$ | 6.45     | 5.68                  |
| $\ell = 180^\circ, b = 25^\circ, 2 < d \leq 4$ | 7.55     | 7.28                  |
| $\ell = 180^\circ, b = 25^\circ, 4 < d \leq 6$ | 7.76     | 6.86                  |

corrected scale heights for our sample of Gaia-RV targets are

$$h_{z,\text{thin}}(R) = (0.93 \pm 0.05)h_{z,\text{thin},G<19}(R) \quad (12)$$

$$h_{z,\text{thick}}(R) = h_{z,\text{thick},G<19}(R).$$

### 3.4. Parametrization of vertical velocity rms

The maps of  $\overline{V_z}(R, z)$  are shown in Fig. 1. For the rms,  $\sigma_{V_z}(R, z)$ , which provides a more important component in our calculations, we carry out a fit over the data in order to obtain a smooth function, which reduces the noise in the calculation of its derivative. We carry out fits with a fourth-order polynomial as a function of  $z$  with the linear term in  $z$  set to zero. This functional behavior is chosen as the first derivative of  $\sigma_{V_z}(R, z)$  at  $z = 0$  should be zero (a minimum, given the symmetry for  $z > 0$  and  $z < 0$ ).

Our fits get the following results ( $R, z$  in units of kpc;  $\sigma_{V_z}$  in units of  $\text{km s}^{-1}$ ):

$$\sigma_{V_z}(R, z) = C_0(R) + C_2(R)z^2 + C_3(R)z^3 + C_4(R)z^4. \quad (13)$$

For the anticenter regions, we keep  $C_4 = 0$  and we do an extra fit for each of the coefficients such that

$$C_i(R) = a_{0,i} + a_{1,i}R + a_{2,i}R^2. \quad (14)$$

For the Galactic pole regions, we assume a unique value of  $R = R_\odot$ , so  $a_{1,i}$  and  $a_{2,i}$  are set to zero. The values of the coefficients  $a_{j,i}$  are given in Table 2. The fit of  $\sigma_{V_z}(R = R_\odot, z)$  in the Galactic pole regions is shown in Fig. 2. The fits of  $C_i$  to second-order polynomials in the anticenter regions are given in Fig. 3.

Since the coefficients of the polynomials are correlated, rather than calculating the errors of each coefficient in the fits, we calculate for each value of  $R$  the average deviation (rms) in the whole range of  $z$  of  $\sigma_{V_z}(R, z)$  with respect to the fit of Eq. (13), and we fit it as a function of  $R$ . Given that the errors for the velocities contain an important ratio (unknown) of systematic errors rather than statistical ones alone, the total error is not the error in the fit but somewhat larger. There are two sources of errors: the errors in the fit (statistical) and the errors in each of the measurements of  $\sigma_{V_z}^2$ , which we sum quadratically as a conservative estimation. We assume the error

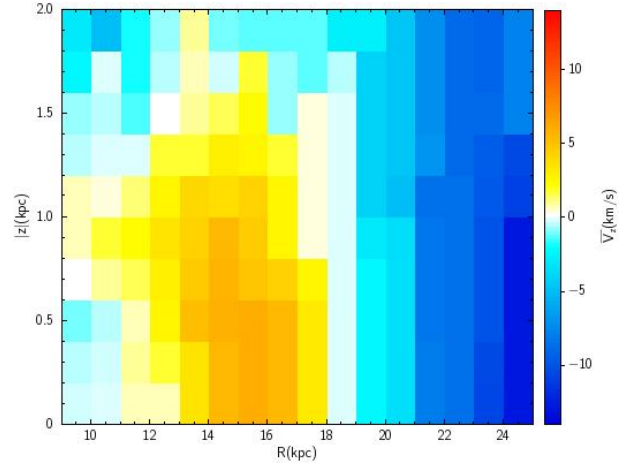
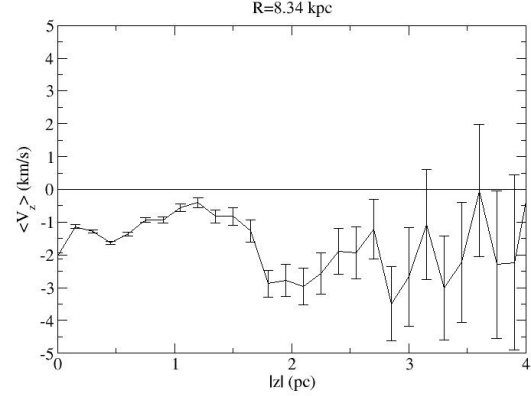


**Figure 1.** Average  $V_z$  from Gaia DR3 extended kinematic maps within the Galactic poles (top panel) and anticenter (bottom panel) lines of sight.

of  $\sigma_{V_z}$  is equal to the quadratic sum of the rms of the fit ( $\sigma_{\text{fit}}$ ) and the average error in each measurement of  $\sigma_{V_z}$ , where

$$\text{Gal. poles : } \sigma_{\text{fit}}[\sigma_{V_z}(R, z)] = \quad (15)$$

$$0.54 - 0.025|z|[\text{kpc}] + 0.043z[\text{kpc}]^2 \text{ km/s}$$

$$\text{Anticenter : } \sigma_{\text{fit}}[\sigma_{V_z}(R, z)] =$$

$$2.89 - 0.341R[\text{kpc}] + 0.0158R[\text{kpc}]^2 \text{ km/s.}$$

We note that this dispersion of vertical velocities corresponds to the rms once subtracted quadratically from the measurement errors in radial velocities and proper motions (López-Corroira & Sylos Labini 2019, Sect. 4), so it reflects the rms of the real distribution of velocities and not the dispersion due to errors in their measurements.

We also show in Fig. 4 the average values of  $\sqrt{|\overline{V_R V_z}|}$ , lower than 8 km/s for the regions to be explored here with significant  $\Sigma$ , most of them even lower than 5 km/s, thus giving that  $|\overline{V_R V_z}| \lesssim 0.04\sigma_{V_z}^2$  (however, in the Galactic pole directions, for  $|z| > 3$  kpc, the values are larger, so we keep the exploration region within  $|z| < 3$  kpc  $\forall R$ ). Hence, and given also that  $h_R \sim (3 - 5) \times h_z$  (see Sect. 4.1), the term in Eq. (4)  $|\overline{V_R V_z}| \left( \frac{1}{h_R} - \frac{1}{R} \right) \lesssim 0.01 \frac{\overline{V_z}^2}{h_z}$

**Table 2**  
Coefficients of the fit in Eqs. (13). Units of  $a_{j,i}$ :  
 $\text{km s}^{-1} \text{kpc}^{-(i+j)}$ .

| $i$             | $a_{0,i}$ | $a_{1,i}$ | $a_{2,i}$ |
|-----------------|-----------|-----------|-----------|
| Galactic poles: |           |           |           |
| 0               | 19.387    | 0         | 0         |
| 2               | 17.862    | 0         | 0         |
| 3               | -8.459    | 0         | 0         |
| 4               | 1.175     | 0         | 0         |
| Anticenter:     |           |           |           |
| 0               | 24.576    | -1.173    | 0.05618   |
| 2               | 8.1905    | -0.023805 | -0.013001 |
| 3               | -2.4622   | 0.060869  | 0.0020495 |

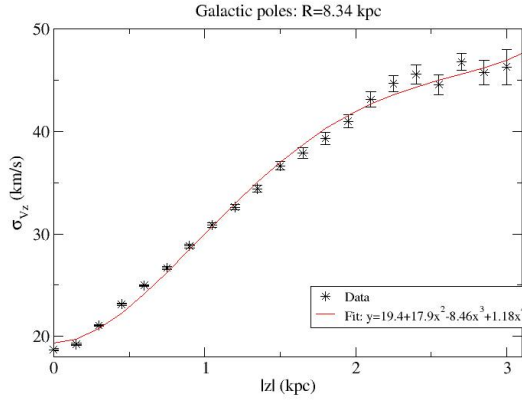


**Figure 2.** Fit of  $\sigma_{V_z}(R = R_\odot, z)$  in the Galactic pole region.

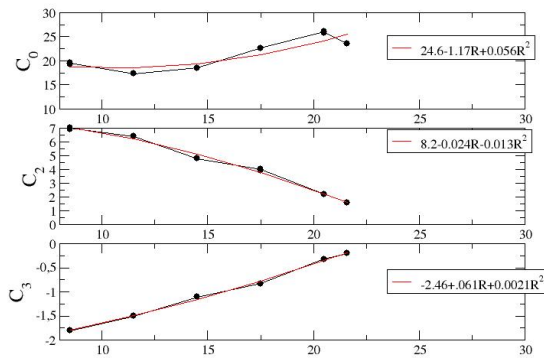


**Figure 3.** Fit of  $C_i$  in the anticenter regions. Units of  $C_i$ :  
 $\text{km s}^{-1} \text{kpc}^{-i}$ .

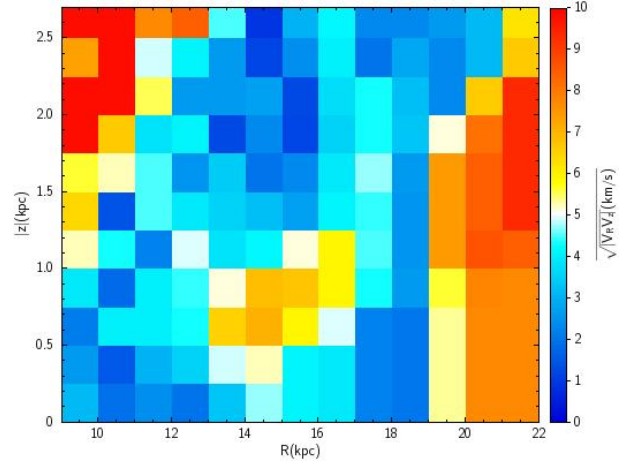
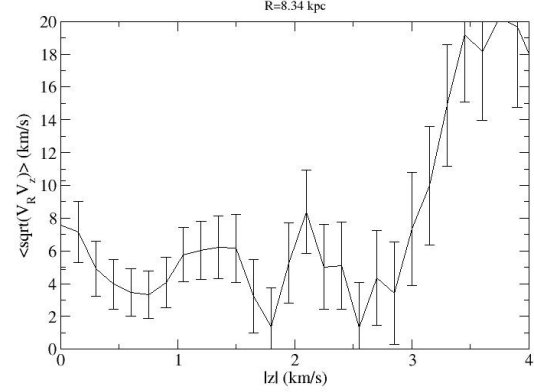


**Figure 4.** Average  $\sqrt{|V_R V_z|}$  from Gaia DR3 extended kinematic maps within the Galactic poles (top panel) and anticenter (bottom panel) lines of sight.

[the dominant term in Eq. (4)]; also the term  $\frac{\partial \overline{V_R V_z}}{\partial R}$  is much smaller than  $\frac{\partial \overline{V_z^2}}{\partial z}$  by a similar ratio. That allows to neglect, as we did in Sect. 2, the terms of  $V_R V_z$  in Eq. (4) since it is two orders of magnitude lower than the contribution of  $\sigma_{V_z}^2$  and error bars are much larger than this small  $\sim 1\%$  relative contribution.

### 3.5. First term of Eq. (8)

From Wang et al. (2023)'s rotation curves, we get  $\beta(z = 0) = -1.7 \pm 0.1 \text{ km s}^{-1} \text{kpc}^{-1}$  for  $R < 25 \text{ kpc}$ , and very small dependence of the slope of rotation curves with  $z$  (Wang et al. 2023, Fig. 10) with variations within 30%, so we can consider  $\beta(z) \approx -1.7 \pm 0.5 \text{ km s}^{-1} \text{kpc}^{-1} \forall z$ . The amplitude of the rotation curve may be modeled as  $V_c(R_\odot, z) \approx 229(1 + \gamma|z|) \text{ km s}^{-1}$ ,  $\gamma \sim -0.03 \pm 0.01 \text{ kpc}^{-1}$  (Wang et al. 2023, Fig. 10).

Therefore, the first term of the right-hand side of Eq. (8) divided by  $4\pi G$  is

$$\Sigma_1(R, z) = \frac{V_c(R_\odot, z) \int_{-z}^z \beta(z') dz'}{2\pi G R} \quad (16)$$

$$\approx -(3.6 \pm 1.1)[z(\text{kpc}) - (0.03 \pm 0.01)z(\text{kpc})^2](R_\odot/R) M_\odot \text{pc}^{-2}.$$

3.6. *Second term of Eq. (8)*

$$\Sigma_2(R, z) = -\frac{1}{2\pi G} \frac{\partial[\overline{V_z^2}(R, z) + \sigma_{V_z}^2(R, z)]}{\partial z} \quad (17)$$

Here, we just need the information on the distribution of vertical velocities we obtained. The errors in the vertical velocity and its rms are calculated as the average in each bin; we do not sum them quadratically because they are dominated by systematic errors rather than statistical ones due to uncertainties in the distance and the application of Lucy's algorithm for the deconvolution of errors. We calculate the derivative of  $\overline{V_z^2}(R, z)$  as the average one on scales  $\Delta z = 150, 300$  and  $450$  pc, in order to reduce the noise; for  $\sigma_{V_z}^2(R, z)$  we use the parameterization obtained in Eqs. (13), (15), which gives ( $R, z$  in units of kpc;  $\sigma_{V_z}$  in units of  $\text{km s}^{-1}$ ):

$$\frac{\partial[\sigma_{V_z}^2(R, z)]}{\partial z} = [4z C_2(R) + 6z^2 C_3(R) + 8z^3 C_4(R)] \sigma_{V_z}(R, z). \quad (18)$$

3.7. *Third term of Eq. (8)*

$$\Sigma_3(R, z) = \frac{\overline{V_z^2}(R, z) + \sigma_{V_z}^2(R, z)}{2\pi G \overline{h_z}(R, z)}. \quad (19)$$

Again, we need information on the distribution of vertical velocities used for the second term, and, moreover, we need information on the flared scale height of the combination of thin and thick disks. The average velocity, which is a minor component, is taken directly from the data. The  $\sigma_{V_z}^2(R, z)$  and its error are taken from the parameterization obtained in Eqs. (13), (15). Eqs. (11), (12) are used to derive the effective scale height  $\overline{h_z}$  in each point through Eq. (10).

3.8. *Results*

In Fig. 5 we show the results of the calculations of  $\Sigma$  for different values of  $R$ . We remind the reader that we are always using the vertical distribution as a sum of two  $\text{sech}^2$  functions (Eq. 7); in the case of  $R = R_\odot$  we also show for comparison the case of vertical distribution as a sum of two exponentials (Eq. 6), in order to illustrate that  $\Sigma$  near the plane is far from zero, which is inconsistent; we should have  $\Sigma(z = 0) = 0$ , with this being the reason to choose  $\text{sech}^2$  functions in the vertical stellar distribution throughout this paper. In Fig. 6, we plot it as a function of both  $R$  and  $z$  in the anticenter volume. Due to geometric issues and the lack of stars, the relative error bars at large  $|z|$  are larger than at low  $|z|$ .

At  $R = R_\odot$ , we get the most significant value of  $\Sigma(R = R_\odot, z = 0.75 \text{ kpc}) = 45 \pm 9 \text{ M}_\odot \text{ pc}^{-2}$ ; for larger  $z$ , the relative error bars become much larger. For instance,  $\Sigma(R = R_\odot, z = 1.05 \text{ kpc}) = 39 \pm 18 \text{ M}_\odot \text{ pc}^{-2}$ . The origin of these large bars mainly stems from the uncertainties of  $\sigma_{V_z}$  and  $\overline{h_z}$ . These results are more or less compatible with other measurements in previous works with similar methods, e.g.,  $\Sigma(R = R_\odot, z = 1 \text{ kpc}) = 78.7_{-4.7}^{+3.9} \text{ M}_\odot \text{ pc}^{-2}$  (Xia et al. 2016);  $\Sigma(R = R_\odot, z = 1.1 \text{ kpc}) = 72_{-9}^{+6} \text{ M}_\odot \text{ pc}^{-2}$  (Horta et al. 2024);  $\Sigma(R = R_\odot, z = 1.1 \text{ kpc}) =$

$55.5 \pm 1.7 \text{ M}_\odot \text{ pc}^{-2}$  (Nitschai et al. 2021);  $\Sigma(R = R_\odot, z = 1 \text{ kpc}) \approx 65 \text{ M}_\odot \text{ pc}^{-2}$  (Cheng et al. 2024), although we suspect that these much lower error bars are due to the fact those authors have not fully taken into account all of the uncertainties.

At  $R > R_\odot$  in the anticenter, we get results consistent with other independent analyses (Nitschai et al. 2021, Fig. 7), although with much larger error bars:  $\Sigma(R = 10 \text{ kpc}, z = 1.05 \text{ kpc}) = 28.7 \pm 9.6 \text{ M}_\odot \text{ pc}^{-2}$ ;  $\Sigma(R = 13 \text{ kpc}, z = 1.05 \text{ kpc}) = 25.0 \pm 5.7 \text{ M}_\odot \text{ pc}^{-2}$ ;  $\Sigma(R = 16 \text{ kpc}, z = 1.05 \text{ kpc}) = 16.9 \pm 5.8 \text{ M}_\odot \text{ pc}^{-2}$ ;  $\Sigma(R = 19 \text{ kpc}, z = 1.05 \text{ kpc}) = 11.4 \pm 6.6 \text{ M}_\odot \text{ pc}^{-2}$ ;  $\Sigma(R = 22 \text{ kpc}, z = 1.05 \text{ kpc}) = 11.7 \pm 14.9 \text{ M}_\odot \text{ pc}^{-2}$ . Similar numbers were also obtained in Sylos Labini (2024, Fig. 11/top panel) (note that  $a_z = 2\pi G \Sigma$ ) using the same data with an independent calculation.

Guo et al. (2024) proposed a model-independent method to measure the vertical potential utilizing the intersections between the vertical phase space ( $V_z$  vs.  $z$ ), assuming that the vertical and in-plane motions are separable and the vertical energy per unit mass of the derived intersections of the phase-space snail is conserved and connected with potential of the Galaxy. They measure the intersections of the phase-space snail within  $7.6 < R < 11.1 \text{ kpc}$  for Gaia DR3, and apply the interpolation method to deduce the potential values at several vertical heights. According to them,  $\Sigma(R_\odot, z) \approx 25, 35, 50, 75 \text{ M}_\odot/\text{pc}^2$  for  $z = 0.15, 0.30, 0.60, 1.05 \text{ kpc}$  respectively (Guo et al. 2024, Fig. 12/bottom panel). They are similar trends of  $\Sigma(z)$  to our results, although with slightly larger amplitude.

3.9. *Reliability of the error bars*

Although the results we obtain are roughly comparable with others obtained in the literature, we get much larger error bars. Let us understand why the error bars are so large with an analysis for one of the values of  $\Sigma$ ; for other values of  $R, z$  the analysis would be similar.

For instance, for  $R = 10 \text{ kpc}, z = 1.05 \text{ kpc}$ , we get  $\Sigma = 28.7 \pm 9.6 \text{ M}_\odot \text{ pc}^{-2}$ . For this bin, the three terms of Eq. (8) are:  $\Sigma_1 = -3.1 \pm 1.0 \text{ M}_\odot \text{ pc}^{-2}$ ,  $\Sigma_2 = -14.8 \pm 1.2 \text{ M}_\odot \text{ pc}^{-2}$ ,  $\Sigma_3 = 46.6 \pm 9.4 \text{ M}_\odot \text{ pc}^{-2}$ . Clearly, the error bar of  $\Sigma$  is dominated by the error in  $\Sigma_3$ , which is mainly produced by the error in  $\overline{h_z}(R = 10 \text{ kpc}, z = 1.05 \text{ kpc}) = (454 \pm 51) \text{ pc}$  and the error in  $\sigma_{V_z} = 23.9 \pm 1.7 \text{ km/s}$ ; the contribution of  $V_z$  is negligible. A relative error in  $\sigma_{V_z}$  of 7% makes an error of 14% in  $\sigma_{V_z}^2$ , which, together with the error of 11% in  $\overline{h_z}$ , makes the error of  $\Sigma_3 \approx 20\%$ .

Why is the relative error of  $\overline{h_z}$  11%? There are three sources of error in  $\overline{h_z}$ : (1) the error in  $h_{z,\text{thin}} = 254 \pm 44 \text{ pc}$ : this produces a relative error in  $\overline{h_z}$  of 1.8%; (2) the error in  $h_{z,\text{thick}} = 810 \pm 200 \text{ pc}$ : this produces a relative error in  $\overline{h_z}$  of 10.4%; and (3) the error in  $f = 0.09 \pm 0.01$ : this produces a relative error in  $\overline{h_z}$  of 4.1%.

## 4. DARK MATTER DENSITY

4.1. *Visible matter*

The total density is the sum of the visible baryonic component ( $\rho_{\text{vis}}$ ) plus the dark matter (either baryonic or non-baryonic) component ( $\rho_{\text{dark}}$ ). A good knowledge of the visible matter is important to ascertain the amount of

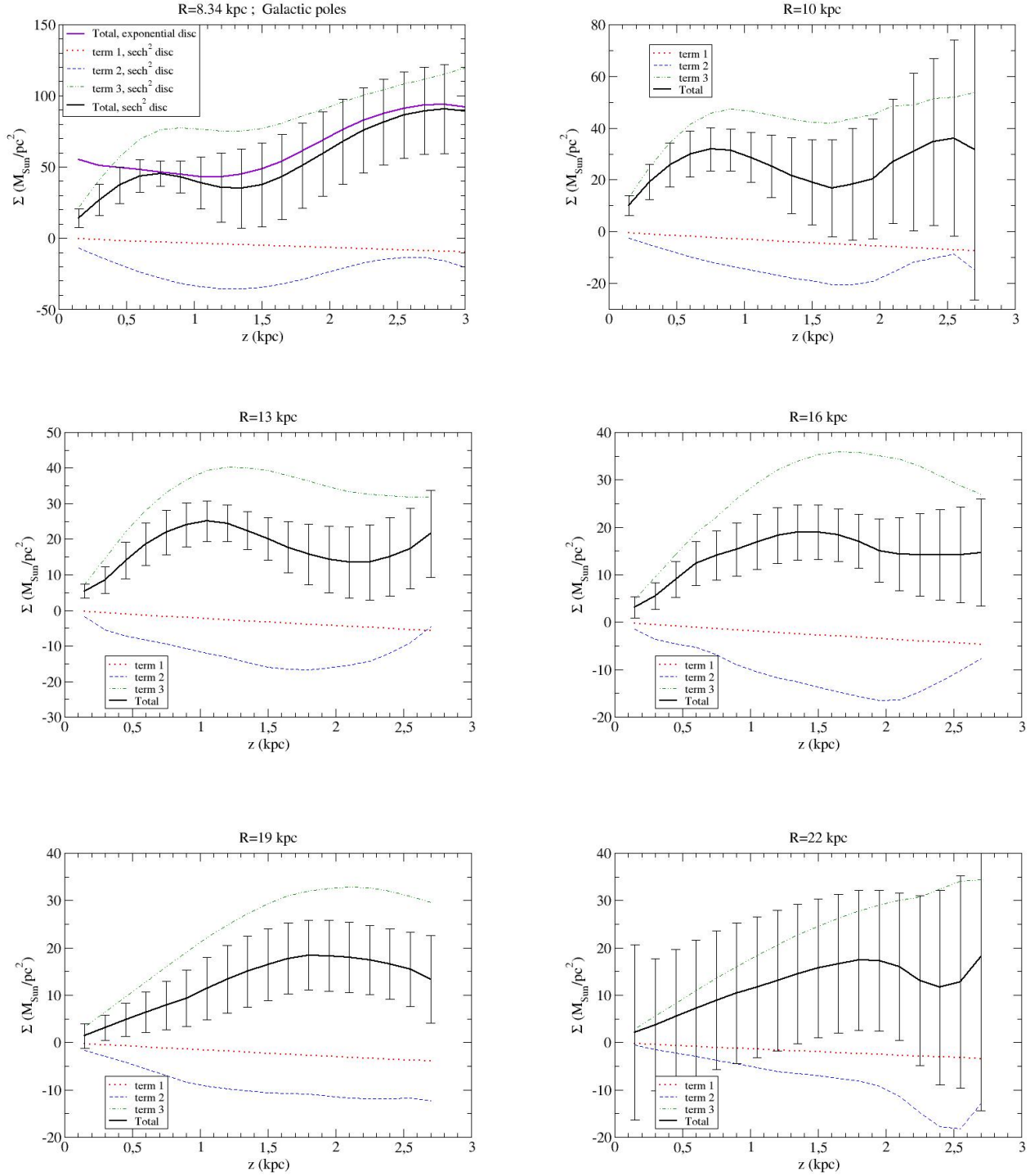


**Figure 5.** Surface density as a function of maximum  $z$  for different  $R$ . Terms 1, 2 and 3 stand for the three terms ( $\Sigma_1$ ,  $\Sigma_2$  and  $\Sigma_3$ ) that sum the total surface density. The plot of  $R = R_{\odot} = 8.34$  kpc corresponds to the Galactic pole regions; the rest of them are from the anticenter region. Bins with  $\Delta z = 0.15$  kpc;  $\Delta R = 1$  kpc (anticenter),  $\Delta R = 2$  kpc (Galactic poles). Sech<sup>2</sup> vertical density distribution for thin/thick disks except for  $R = R_{\odot}$  where we also plot  $\Sigma$  for exponential vertical density.



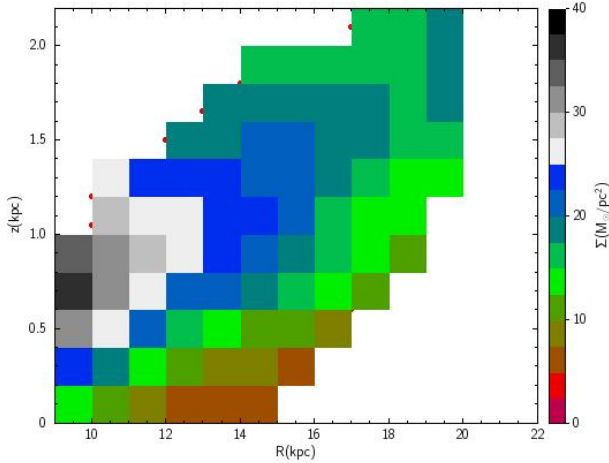


**Figure 6.** Surface density as a function of maximum  $z$  and  $R$  in the anticenter. Bins with  $\Delta R = 1$  kpc,  $\Delta z = 0.15$  kpc. Only bins with signal/noise larger than two are plotted.

dark matter using velocity dispersions (Hessman 2015). The stellar mass density is proportional to the stellar density of the disk given in Eq. (7), neglecting the stellar halo contribution in the given range of  $R$  and  $z$ , and we must add a new term for gas+dust:

$$\rho_{\text{vis.}}(R, z) = \rho_{M,*,\odot} \exp\left(-\frac{R - R_\odot}{h_R}\right) \quad (20)$$

$$\times \left[ (1 - f) \text{sech}^2\left(\frac{|z|}{2h_{z,\text{thin}}(R)}\right) + f \text{sech}^2\left(\frac{|z|}{2h_{z,\text{thick}}(R)}\right) \right]$$

$$+ \rho_{M,\text{gas+dust},\odot} \exp\left(-\frac{R - R_\odot}{h_{R,\text{gas}}}\right) \text{sech}^2\left(\frac{|z|}{2h_{z,\text{gas}}(R)}\right)$$

with the same ratio of 'thick disk'/'total disk' stars  $f = 0.09 \pm 0.01$  (Chrobáková et al. 2022), stellar scale length  $h_R = 2.2 \pm 0.1$  kpc (Chrobáková et al. 2022), gas scale length  $h_{R,\text{gas}} = 3.15 \pm 0.60$  kpc (Kalberla & Dedes 2008) (error estimated by the dispersion on the dependence with azimuth), the stellar scale heights given by Eqs. (11) and (12), and for the gas we assume the one derived for the HI (dominant component of gas) by Kalberla & Dedes (2008) (error estimated by the dispersion north/south):

$$h_{z,\text{gas}} = (0.15 \text{ kpc}) \exp\left(\frac{R - R_\odot}{h_{R,fg}}\right), \quad (21)$$

$$E_{h_{z,\text{gas}}}(R) = 0.2 h_{z,\text{gas}},$$

$E_{h_{z,\text{gas}}}$  stands for the error in  $h_{z,\text{gas}}$ ;  $h_{R,fg} = 9.8$  kpc, and the normalizations in the solar neighborhood are  $\rho_{M,*,\odot} = 0.033 \pm 0.003 \text{ M}_\odot/\text{pc}^3$ ,  $\rho_{M,\text{gas},\odot} = 0.023 \pm 0.003 \text{ M}_\odot/\text{pc}^3$  in order to get (McKee et al. 2015)

$$\Sigma_{M,*,\odot}(R_\odot, z = \infty) = 4\rho_{M,*,\odot} [(1 - f)h_{z,\text{thin}}(R_\odot) \quad (22)$$

$$+ f h_{z,\text{thick}}(R_\odot)] = (33.4 \pm 3.0) \text{ M}_\odot/\text{pc}^2,$$

$$\Sigma_{M,\text{gas+dust},\odot}(R_\odot, z = \infty) = 4\rho_{M,\text{gas+dust},\odot} h_{z,\text{gas}}(R_\odot) \quad (23)$$

$$= (13.7 \pm 1.6) \text{ M}_\odot/\text{pc}^2.$$

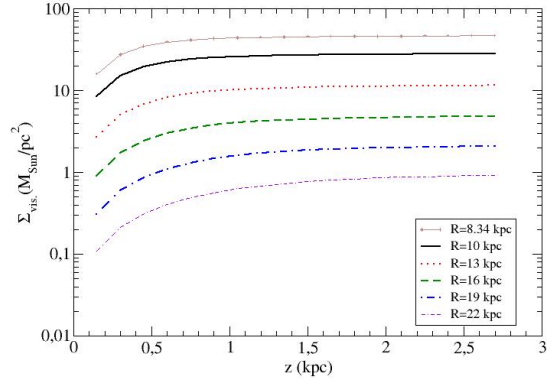


**Figure 7.** Prediction of visible matter component of surface density as a function of maximum  $z$  for different  $R$ .

Errors in  $\rho_{M,\odot}$  only take account the errors of  $\Sigma_{M,\odot}(R_\odot, z = \infty)$ . This makes a total density of visible matter in the solar neighborhood of  $0.056 \pm 0.005 \text{ M}_\odot/\text{pc}^3$  for a  $\text{sech}^2$  vertical distribution, equivalent to double it,  $0.112 \pm 0.010 \text{ M}_\odot/\text{pc}^3$  if we assumed an exponential vertical distribution. Other independent estimations give a similar value: for instance,  $0.098^{+0.006}_{-0.014} \text{ M}_\odot/\text{pc}^3$  (Garbari et al. 2012) with an exponential vertical distribution.

We can see the contribution of visible matter to the surface density ( $\Sigma_{\text{vis.}}(R, z) \equiv \int_{-z}^z \rho_{\text{vis.}}(R, z') dz'$ ) in Fig. 7.

#### 4.2. Calculation of dark matter density

With this, we can calculate the dark matter density as a function of  $R$  and  $z$  as

$$\rho_{\text{dark}}(R, z) = \frac{1}{2} \frac{\partial [\Sigma(R, z) - \Sigma_{\text{vis.}}(R, z)]}{\partial z}, \quad (24)$$

or for some range with  $|z|$  between  $z_1$  and  $z_2$ ,

$$\bar{\rho}_{\text{dark}}(R, z_1 < z < z_2) = \quad (25)$$

$$\frac{1}{2} \frac{[\Sigma(R, z_2) - \Sigma_{\text{vis.}}(R, z_2) - \Sigma(R, z_1) + \Sigma_{\text{vis.}}(R, z_1)]}{z_2 - z_1}.$$

Figure 8 shows the outcome for  $z_1 = 0$ ,  $z_2 = 150$ , 1050 pc;  $z_1 = 1050$  pc,  $z_2 = 2100$  pc;  $z_1 = 2100$  pc,  $z_2 = 2700$  pc.

Given the large error bars, the data are almost compatible with the total absence of dark matter. We get an average density for  $R = R_\odot$  and within  $|z| < 0.15$  kpc:  $\langle \rho_{\text{dark}} \rangle (R = R_\odot, |z| < 0.15 \text{ kpc}) = -0.010 \pm 0.022 \text{ M}_\odot \text{ pc}^{-3}$ . Why do we get a negative value of the dark matter density? Because the model of visible matter has an amplitude larger than the total amplitude, we have a total  $\langle \rho_{\text{total}} \rangle (R = R_\odot, |z| < 0.15 \text{ kpc}) = 0.047 \pm 0.021 \text{ M}_\odot \text{ pc}^{-3}$  and  $\langle \rho_{\text{vis.}} \rangle (R = R_\odot, |z| < 0.15 \text{ kpc}) = 0.056 \pm 0.005 \text{ M}_\odot \text{ pc}^{-3}$ . Nonetheless, as discussed throughout the paper, there are many uncertainties, and we are assuming a  $\text{sech}^2$  vertical distribution, which gives a factor of two lower local density than an exponential distribution, and therefore, a value of  $0.08\text{--}0.10 \text{ M}_\odot \text{ pc}^{-3}$  for

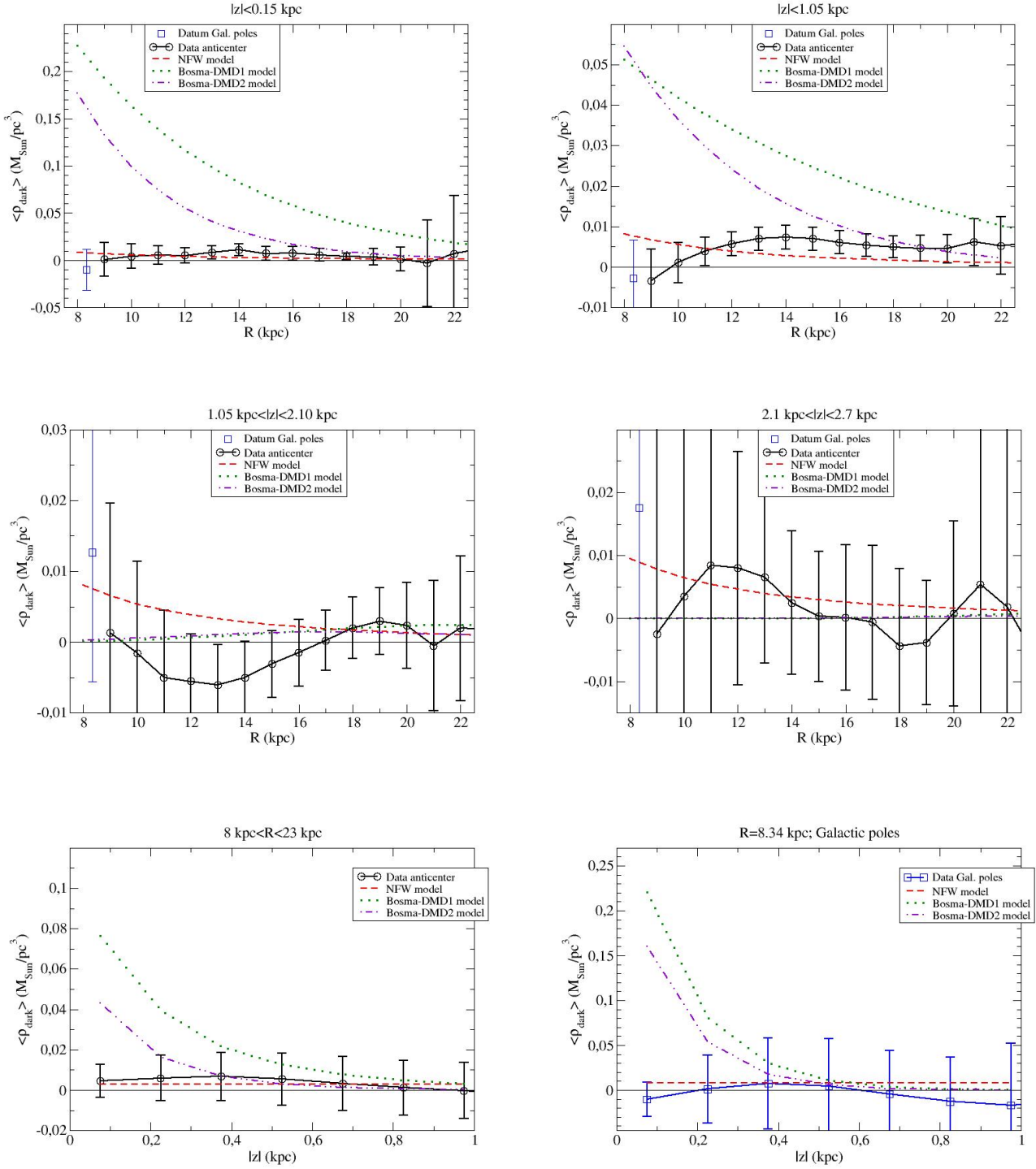


**Figure 8.** Average dark matter density derived from Eq. (25). Error bars include both the errors in the data and the errors in the visible matter model. Top left: average within  $|z| < 0.15$  kpc, as a function of  $R$ . Top right: average within  $|z| < 1.05$  kpc, as a function of  $R$ . Middle left: average within  $1.05 \text{ kpc} < |z| < 2.10$  kpc, as a function of  $R$ . Middle right: average within  $2.1 \text{ kpc} < |z| < 2.7$  kpc, as a function of  $R$ . Bottom left: average within  $8 \text{ kpc} < R < 23$  kpc, as a function of  $|z|$  within  $|z| < 1.05$  kpc in the anticenter region. Bottom right: average density at  $R = 8.34$  kpc, as a function of  $|z|$  within  $|z| < 1.05$  kpc in the Galactic pole regions. Comparison with theoretical models.

the total density in the solar neighborhood, as measured by other groups (McKee et al. 2015; Horta et al. 2024), assuming an exponential distribution, cannot be excluded. Indeed, we note that in our calculations with an exponential distribution instead of  $\text{sech}^2$  the value of  $\langle \rho_{\text{total}} \rangle (R = R_{\odot}, |z| < 0.15 \text{ kpc})$  would rise to  $0.184 M_{\odot} \text{ pc}^{-3}$ , so possibly some intermediate distribution between exponential and  $\text{sech}^2$  would get better values.

Again, these large error bars reflect the large uncertainties in the input parameters of the velocity dispersion and scale height, and also the uncertainties in the models of visible matter. The bins of the Galactic anti-center are less noisy than the ones at the Galactic poles, and for  $R$  between 13 and 16 kpc we get the most significant results. The hypothesis of zero dark matter [ $\rho_{\text{dark}}(R, z) = 0 \forall R, z$ ] is not far from the data. At present, exploring the different values of  $R, z$ , the most significant departure from  $\rho_{\text{dark}}(R, z) = 0$  is only at  $2.6\sigma$ :  $\langle \rho_{\text{dark}} \rangle (R = 14 \text{ kpc}, |z| < 1.05 \text{ kpc}) = (7.4 \pm 2.9) \times 10^{-3} M_{\odot} / \text{pc}^3$ .

#### 4.3. Comparison with dark matter models

From the rotation curves at  $z = 0$  derived from the same data of Gaia DR3 with Lucy deconvolution of errors, there are two possible solutions for the dark matter distribution (Sylos Labini et al. 2023):

1. A spherical distribution with a Navarro-Frenk-White (NFW) profile:

$$\rho_{\text{dark,sph}}(R, z) = \frac{\rho_{ds0}}{\left(1 + \frac{\sqrt{R^2+z^2}}{r_s}\right)^2 \frac{\sqrt{R^2+z^2}}{r_s}}, \quad (26)$$

with best-fit parameters (Sylos Labini et al. 2023, Table 2/DR3+):  $\rho_{ds0} = 0.014 M_{\odot} / \text{pc}^3$ ,  $r_s = 12.6 \text{ kpc}$ . This value of the density of dark matter in the solar neighborhood,  $\rho_{ds0}$ , is similar to the values obtained by different teams: for instance,  $0.022_{-0.013}^{+0.015} M_{\odot} / \text{pc}^3$  (Garbari et al. 2012): from Milky Way rotation curve implies  $\rho_{ds0} = 0.4 \text{ GeV}/c^2 \text{ cm}^{-3} = 0.011 M_{\odot} \text{ pc}^{-3}$  (Catena & Ullio 2012; Pato et al. 2015; de Salas & Widmark 2021; Ou et al. 2024);  $0.018 \pm 0.0054 M_{\odot} \text{ pc}^{-3}$  (Xia et al. 2016). These parameters were derived assuming a more simple expression of visible matter, which we use here, and  $\rho_{ds0}$ ,  $r_s$  may slightly change for a fit of the rotation curve using Eqs. (20) instead, but these variations are small and do not affect our analysis, which, as said below, tries to determine whether this NFW profile is compatible with the data with some error bars much larger than these small changes due to different fits of the rotation curve.

2. A disky distribution of dark matter tracing the gas (Bosma 1981; Sylos Labini et al. 2023):

[DMD1:]

$$\Sigma_{\text{dark,disc}}(R, \infty) = \Sigma_{dd0} \exp\left(-\frac{R}{R_d}\right), \quad (27)$$

with best-fit parameters (Sylos Labini et al. 2023, Table 3/DR3+):  $\Sigma_{dd0} = 230 M_{\odot} / \text{pc}^2$ ,  $R_d = 10.2$

kpc. We can assume a vertical exponential distribution; thus,

$$\rho_{\text{dark,disc}}(R, z) = \frac{\Sigma_{dd0}}{2h_{z,\text{dark}}(R)} \exp\left(-\frac{R}{R_d}\right) \times \exp\left(-\frac{|z|}{h_{z,\text{dark}}(R)}\right). \quad (28)$$

We assume that  $h_{z,\text{dark}}(R) = h_{z,\text{gas}}(R)$  given by Eq. (21). Hereafter, we refer as DMD1 this model with these parameters.

[DMD2:] The last parameters were obtained from rotation curves with simpler than the assumptions herein about the visible matter. If we used the same model of visible matter that we used here, Eq. (20), in the fit of the rotation curve, and also assuming  $\text{sech}^2$  vertical distribution of dark matter, we would get

$$\rho_{\text{dark,disc}}(R, z) = \frac{\Sigma_{dd0}}{4h_{z,\text{dark}}(R)} \exp\left(-\frac{R}{R_d}\right) \times \text{sech}^2\left(\frac{|z|}{2h_{z,\text{dark}}(R)}\right), \quad (29)$$

with  $\Sigma_{dd0} = 570 M_{\odot} / \text{pc}^2$ ,  $R_d = 5.0 \text{ kpc}$  (Sylos Labini, priv. comm. 2024; Sylos Labini (2024) obtains the same values for an exponential vertical distribution too). Again, we assume that  $h_{z,\text{dark}}(R) = h_{z,\text{gas}}(R)$  given by Eq. (21). Hereafter we refer as DMD2 this model with these parameters.

Figs. 8 and 9 show the expected average  $\rho$  or  $\Sigma$  of the NFW model and the Bosma models (DMD1 or DMD2).

Visually examining Fig. 8, the NFW model is compatible with the data.

The disky dark matter model is not compatible with the data when we assume the dark matter is proportional to the gas, as originally proposed by Bosma. A disky dark matter would need a much higher scale height. Taking the data with the measurements at  $R_{\odot}$ ,  $|z| < 0.15 \text{ kpc}$ , and comparing them with Eq. (28) or (29) with  $h_{z,\text{dark}}(R)$  as free parameter for each  $R$ , we get the minimum scale heights compatible with the data within  $1\sigma$ - $5\sigma$ . They are plotted in Fig. 10. We can see that, even assuming a  $2\sigma$  deviation in  $\rho_{\text{dark}}(R, |z| < 0.15 \text{ kpc})$ , we need  $h_{z,\text{dark}} > 600 \text{ pc}$  for  $8 \text{ kpc} < R < 12 \text{ kpc}$  in the best of the cases (DMD2). Such a large thickness is very different from the scale height of the gas equal to  $150 \text{ pc}$  at  $R_{\odot}$  as expected from the Bosma hypothesis.

## 5. CALCULATIONS WITH MOND

The calculation with MOND, which posits a Galaxy only with visible matter (without dark matter component) and with modifications to the gravity, differs from the previous analysis in the variation of the Poisson equation, which now becomes (Bekenstein & Milgrom 1984; López-Corredoira & Betancort-Rijo 2021; Zhu et al. 2023)

$$4\pi G\Sigma(R, z) = \frac{1}{R} \int_{-z}^z \frac{\partial[Ra_R(R, z)\mu(R, z)]}{\partial R} dz' \quad (30)$$

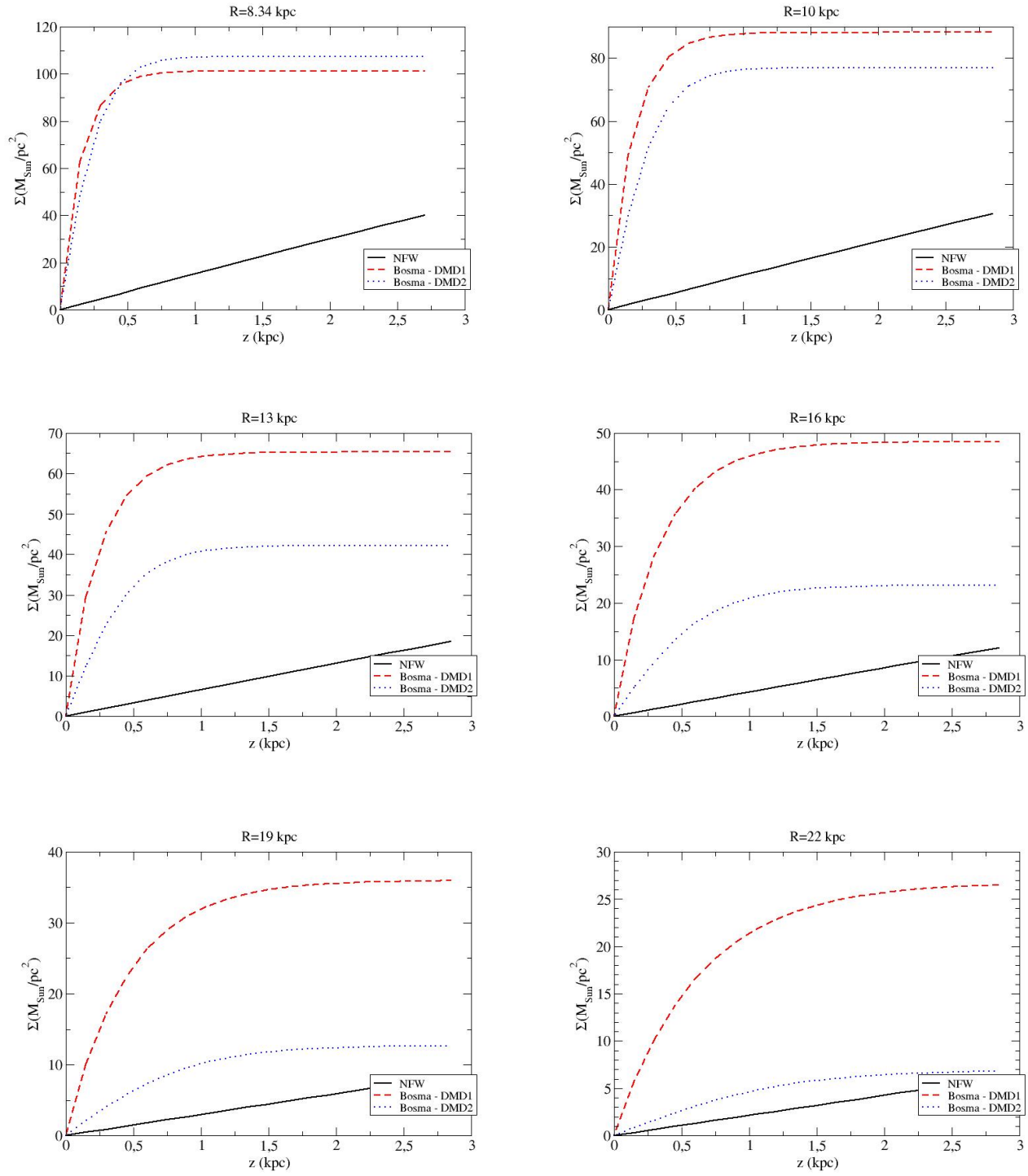


**Figure 9.** Predicted dark matter surface density as a function of maximum  $z$  for different  $R$  from the models of spherical distribution with an NFW profile and disk distribution of dark matter assuming a scale height like that of the gas.

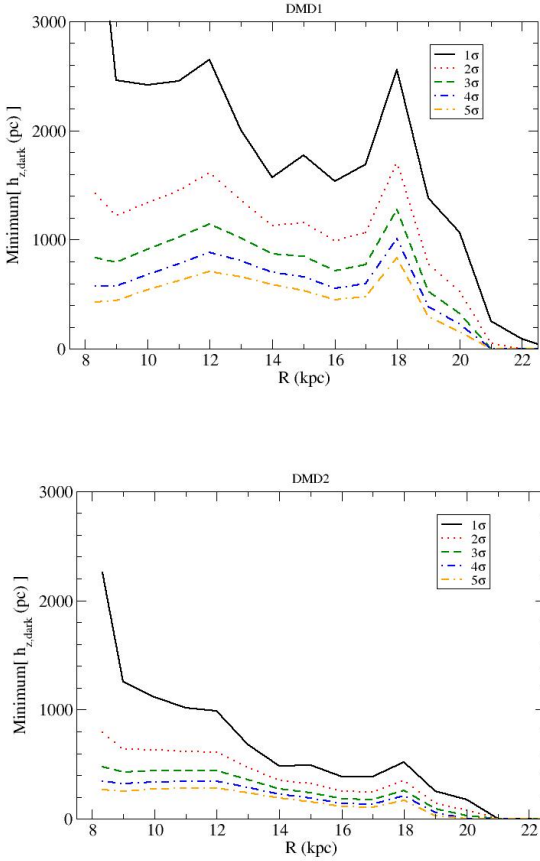


**Figure 10.** Minimum scale height of a disk distribution of dark matter compatible with the data within  $1\sigma$ - $5\sigma$ . Top panel: DMD1 model; bottom panel: DMD2 model

$$+ [a_z(R, z)\mu(R, z) - a_z(R, -z)\mu(R, -z)],$$

$$\mu(R, z) = \left[ 1 + \frac{a_0^2}{a_R(R, z)^2 + a_z(R, z)^2} \right]^{-1/2},$$

where  $a_0 = 1.2 \times 10^{-10} \text{ m s}^{-2}$ ; and setting  $\rho_{\text{dark}}(R, z) = 0 \forall R \forall z$ . We develop this expression as we did in section 2, considering here the approximation of  $\beta = 0$  (flat rotation curve). We have seen in previous sections that the first term of  $\Sigma(R, z)$  of Eq. (8) gives a negligible contribution given the low value of  $\beta$ , so we can neglect it: For instance, this term gives a contribution for  $\Sigma(z = 1 \text{ kpc}) = 3.5 \frac{R_\odot}{R} M_\odot/\text{pc}^2$ , which is much smaller than the error bars, ranging between  $16 M_\odot/\text{pc}^2$  for  $R = R_\odot$  to a minimum of  $5.3 M_\odot/\text{pc}^2$  for  $R = 16 \text{ kpc}$ , so it is always lower than  $1/3$  of the total error bar. Neglecting the term with  $\beta$  should thus produce a systematic error lower than  $1/3$  of the total errors of other terms, which can be considered negligible. With this one and previous approximations we get

$$4\pi G \Sigma(R, z) \approx \frac{V_c(R_\odot, z)^2}{R} \int_{-z}^z \frac{\partial \mu(R, z')}{\partial R} dz' \quad (31)$$

$$-2\mu(R, z) \frac{\partial \overline{V_z^2}(R, z)}{\partial z} + 2\mu(R, z) \frac{\overline{V_z^2}(R, z)}{h_z(R, z)},$$

$$\mu(R, z) = \left[ 1 + \frac{a_0^2}{\frac{V_c(R_\odot, z)^4}{R^2} + \left[ -\frac{\partial \overline{V_z^2}(R, z)}{\partial z} + \frac{\overline{V_z^2}(R, z)}{h_z(R, z)} \right]^2} \right]^{-1/2}.$$

The factor  $\mu$  depends only on the acceleration, and it can be derived directly from kinematics data. In Fig. 11, we show its value. In Fig. 12, we give the calculation of  $\Sigma(R, z)$  for MOND. The first term is again small. We are within a moderate MONDian regime of  $\mu \gtrsim 0.6$  for  $R < 20 \text{ kpc}$ , where  $\Sigma_{\text{MOND}}(R, z) \approx \Sigma_{\text{Newton}}(R, z)\mu(R, z)$ , which gives a decrease in the density lower than 67% with respect to the Newtonian one.

Given that  $\Sigma(R, z) = \Sigma_{\text{vis}}(R, z)$  (there is no dark matter), one would expect that  $\Sigma(R, z)$  in Fig. 12 were the same as those given in Fig. 7. We get that. Fig. 13 illustrates this agreement. MOND works here.

Recently, Chan & Law (2023) claimed that MOND is rejected at  $5\text{-}\sigma$  level in the fit of the rotation curve of Milky Way at  $R=17\text{-}23 \text{ kpc}$ . However, other analyses (Chrobáková et al. 2020; Wang et al. 2023; Sylos Labini et al. 2023) have shown that MOND may fit the rotation curve within the uncertainties, and as we have seen here, the distribution of vertical velocities is also compatible with MOND and the visible (baryonic) matter knowledge. Eq. (8) of Chan & Law (2023) assumes that the rotation curve with MOND is the rotation curve with baryon matter multiplied by a factor of  $1/\sqrt{\mu}$ , an approximation that must be reconsidered when we try to fit data with small error bars. Indeed, a declining rotation curve rather than a flat one is not incompatible with MOND (López-Corredoira & Betancort-Rijo 2021). In any case, rotation curves are not the topic of this paper, but the dispersion of vertical velocities, which present no problem with MOND within the error bars.

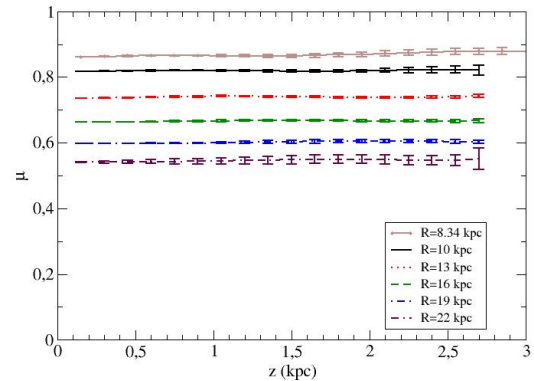


**Figure 11.** Factor  $\mu$  in MOND equations derived from the kinematical data.

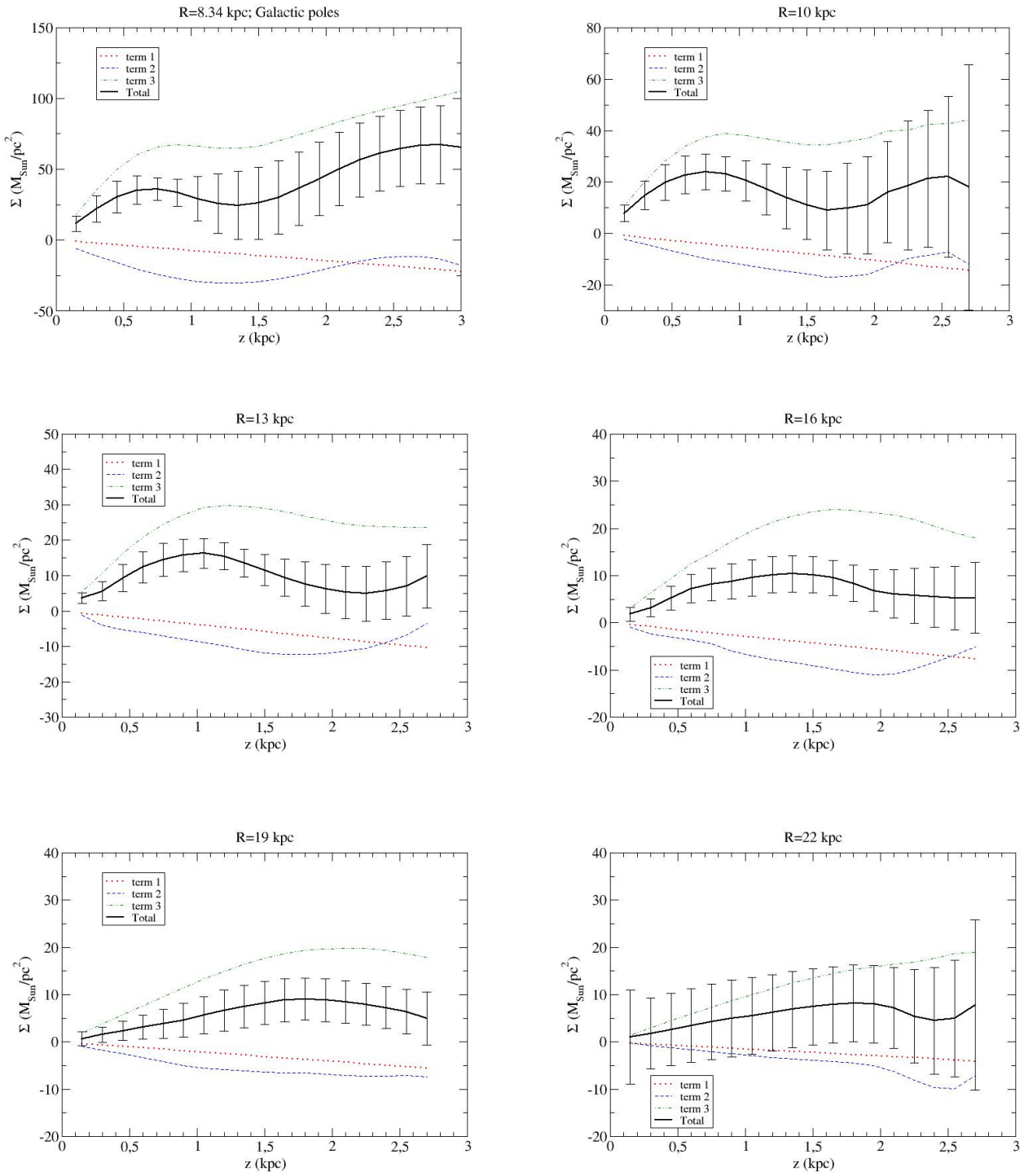


**Figure 12.** Surface density as a function of maximum  $z$  for different  $R$  with MOND. Terms 1, 2, 3 stand for the three terms that sum the total surface density in Eq. (31). The plot of  $R = 8.34$  kpc corresponds to the Galactic pole regions; the rest of them are from the anticenter region. Bins with  $\Delta z = 0.15$  kpc;  $\Delta R = 1$  kpc (anticenter),  $\Delta R = 2$  kpc (Galactic poles).

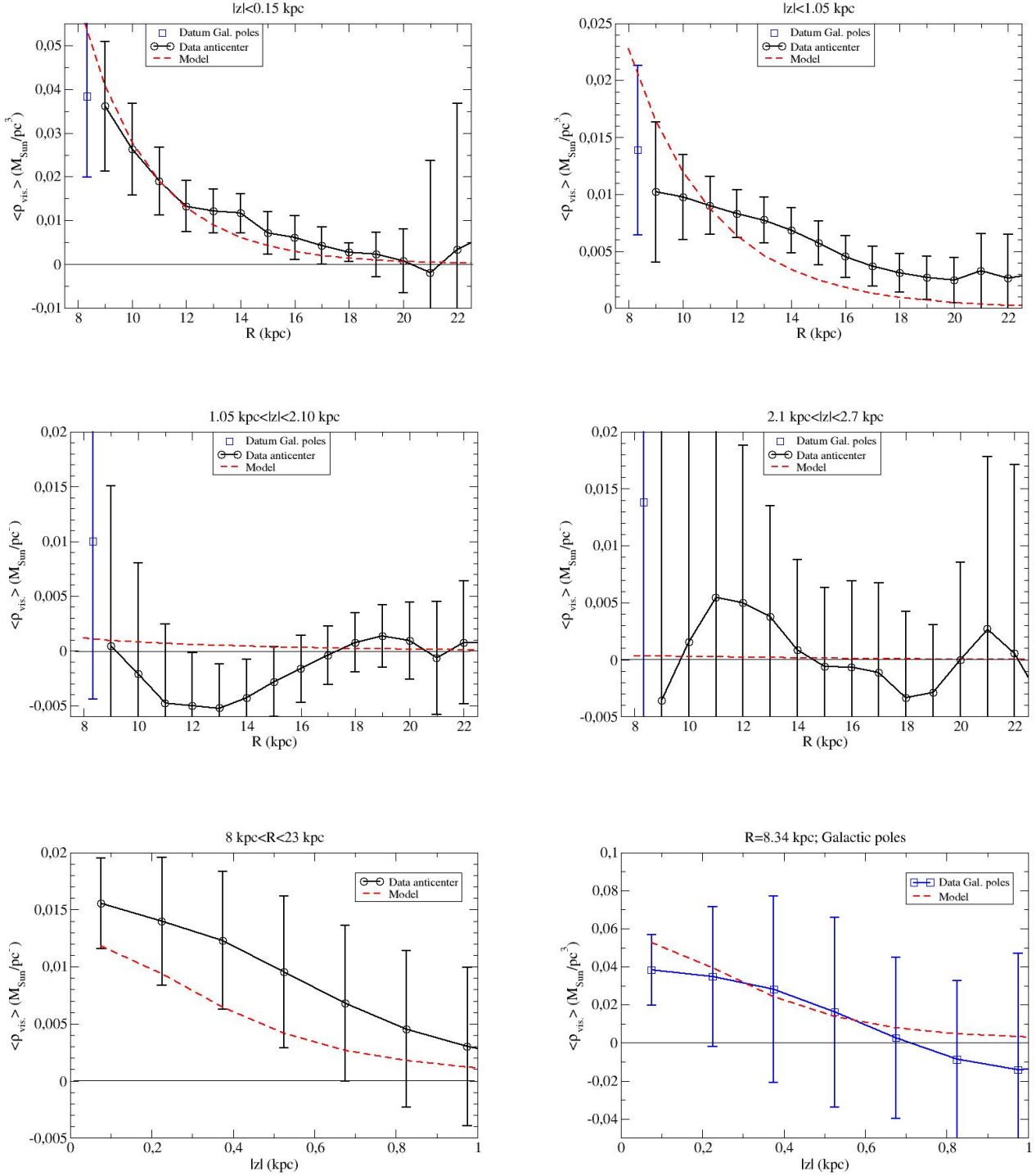


**Figure 13.** Average visible matter density assuming MOND, in comparison with the model of visible matter. Top left: average within  $|z| < 0.15$  kpc, as a function of  $R$ . Top right: average within  $|z| < 1.05$  kpc, as a function of  $R$ . Middle left: average within  $1.05 < |z| < 2.10$  kpc, as a function of  $R$ . Middle right: average within  $2.1 < |z| < 2.7$  kpc, as a function of  $R$ . Bottom left: average within  $8 \text{ kpc} \leq R \leq 23$  kpc, as a function of  $|z|$  within  $|z| < 1.05$  kpc in the anticenter region. Bottom right: average density at  $R = 8.34$  kpc, as a function of  $|z|$  within  $|z| < 1.05$  kpc in the Galactic pole regions.

The results of our analyses can be summarized as follows: (i) the model of spherical dark matter halos of NFW and MOND model compatible with the data; (ii) the model of the disk dark matter with density proportional to gas one (Bosma model) is totally excluded by the data [unless the scale height at  $R < 12$  kpc is larger than 600 pc ( $2\sigma$ )]; and (iii) the total lack of dark matter (there is only visible matter) within Newtonian gravity is not very far from the data (only a  $2.6\sigma$  departure at  $R = 14$  kpc).

All of these results depend basically on four measurements or assumptions: the consideration that the Jeans equations are applicable here, assuming equilibrium; the dispersion of the vertical velocities; the average scale height of stellar distribution; and the vertical stellar density distribution near the Galactic plane ( $\text{sech}^2$  or exponential). We will discuss these points in the next subsections.

### 6.1. Applicability of the Jeans equations

In this study, we have assumed that the stellar populations are in dynamical equilibrium, so that we can neglect the partial time derivatives in our theoretical framework, as is commonly done in these types of analyses (Boyd & Tremaine 2012; Moni Bidin et al. 2012b; 2015; Cheng et al. 2024). There may be some factors contributing to a time dependence, but the disequilibrium is negligible in the solar neighborhood (Cheng et al. 2024, §5.4) and the equilibrium necessary to apply the Jeans equations is suitable within  $R \lesssim 20$  kpc (Chrobáková et al. 2020; Koop et al. 2024) within errors lower than 10%. Nonequilibrium may have an effect but as a secondary contribution that is not expected to significantly change the qualitative results. At  $R < 14$  kpc, where the most significant measurements are obtained, the uncertainty due to the application of the Jeans equations is less than 2% (Koop et al. 2024).

### 6.2. Reliability of the dispersion of vertical velocities

Our results are very dependent on the measurement of  $\sigma_{V_z}(R, z)$  in Eq. (13). As said previously, this dispersion of vertical velocities corresponds to the rms once subtracted quadratically the measurement errors in radial velocities and proper motions (López-Corredoira & Sylos Labini 2019, Sect. 4), so it reflects the rms of the real distribution of velocities, and not the dispersion due to errors in their measurements. Independent calculations (Gaia Collaboration 2018; Nitschai et al. 2021; Drimmel et al. 2023; Cheng et al. 2024) give very similar results in the common range ( $R < 14$  kpc).

There is no assumption here, no theoretical priors, but just an analysis of Gaia data. For the least distant sources ( $R \lesssim 14$  kpc), the calculation of this dispersion is just the result of the direct derivation of the distribution of velocities obtained with the component perpendicular to the plane of the proper motions (and a small component of radial velocities in off-plane regions) for the anticenter regions, and the radial heliocentric velocities (and a small component of proper motions) for the Galactic pole regions. Assuming the measurements of Gaia DR3 are correct, the result cannot be changed. For the most distant sources ( $R \gtrsim 14$  kpc), Lucy's method of deconvolution of parallax errors (López-Corredoira &

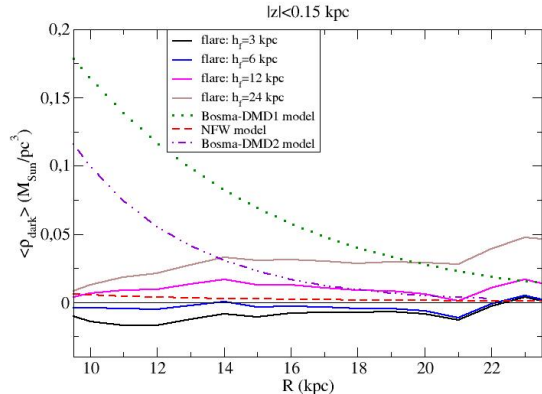


**Figure 14.** Average dark matter density in the anticenter regions with Newtonian gravity within  $|z| < 0.15$  kpc, assuming a scale height with a flare given by Eq. (32), where  $h_f$  is a free parameter (lower  $h_f$ , stronger flare). For comparison, we show the predictions of the models of dark matter discussed in this paper.

Sylos Labini 2019) provides a correction to the statistical real distribution of distance. In principle, all sources of errors in the calculation of distance errors with this method have been taken into account, so there is no reason to doubt this result. Nonetheless, even if we doubted the validity of the Lucy inversion technique, our conclusions would not change because we see clearly the same conclusions for  $R \lesssim 14$  kpc, where Lucy deconvolution has a negligible effect.

### 6.3. The effect of the flare

Another crucial element is the scale height and its variation with  $R$  (flare). It was derived from purely observational analysis of Gaia data stellar distribution, and it is not dependent on theoretical assumptions. Nevertheless, we may speculate that the scale heights are different for some reason. Instead, we will explore some variations of the flare model to see how it affects our results.

We will use the following modeling of scale heights of the stellar density instead of Eqs. (11) and (12):

$$h_{z,\text{thin}}(R) = 0.20 \exp[(R - R_{\odot})/h_f] \text{ kpc} \quad (32)$$

$$h_{z,\text{thick}}(R) = 0.65 \exp[(R - R_{\odot})/h_f] \text{ kpc},$$

where the normalizations are to be coincident at  $R = R_{\odot}$  with Eqs. (11) and (12), and for simplicity we only have one free parameter,  $h_f$  with the same flare for the thin and thick discs. This type of model is indeed used in some other fits available in the literature (e.g., López-Corredoira et al. 2002b; Li et al. 2019).

In Fig. 14 we can see the effect of the variation of  $h_f$  for the density of dark matter assuming Newtonian gravity. Within the range of  $h_f$  between 3 and 24 kpc, the disagreement with the Bosma model is still very large, whereas the NFW is more or less in agreement with any value of  $h_f$ .

### 6.4. Vertical stellar density distribution near the Galactic plane



We have assumed  $\text{sech}^2$  functions in the vertical-direction stellar density, rather than an exponential one, in order to keep the consistency of  $\Sigma(z=0) = 0$ . Nonetheless, we may explore the results of dark matter if we assume an exponential distribution (note that the normalization is changed in Eq. 20 multiplying  $\rho_{M,*,\odot}$  and  $\rho_{M,gas+dust,\odot}$  by a factor two with respect to the  $\text{sech}^2$  distribution in order to obtain the same surface density at  $z = \infty$ ). The dark matter density for this assumption is plotted in Fig. 15.

The major difference with respect to  $\text{sech}^2$  distribution is for  $|z| < 0.15$  kpc, where an exponential distribution would increase  $\Sigma$  very significantly and consequently make  $\rho_{\text{dark}}$  larger. Nonetheless, the dependence on  $R$  is almost flat, which is still incompatible with the Bosma model (and also incompatible with the NFW model); and the density for  $|z| \gtrsim 0.2$  kpc fails to reproduce the Bosma model too.

The fact we get such a significant difference in the results of dark matter density between exponential and  $\text{sech}^2$  distributions at  $|z| < 0.15$  kpc is precisely due to the differences in both stellar distributions there. The high density of dark matter in the plane regions in comparison with other values at higher  $|z|$  makes no sense, and this reinforces the idea that an exponential stellar distribution should not be used. In any case, it does not solve the problems for the Bosma model either.

## 7. FURTHER DISCUSSION AND CONCLUSIONS

Our analysis applies the Jeans equations to the stellar velocity distribution of Gaia DR3 stars in the anticenter and the Galactic poles to obtain the dynamical mass distribution near the plane regions. With the use of the extended kinematic maps produced with a parallax error deconvolution technique (López-Corredoira & Sylos Labini 2019), we are able to reach distances up to  $R = 22$  kpc. Once we have the total mass density as a function of  $R, z$  (we assume an axisymmetric disk), we subtract the amount due to visible matter, and we obtain dark matter density. Alternatively, substituting Newtonian gravity for MOND gravity, we obtain directly the total density equal to the visible matter density.

This type of analysis has been carried out previously (e.g., Moni Bidin et al. 2012b; Loebman et al. 2012; Villa Durango 2022; Cheng et al. 2024), but not in a way as complete as we did here. Here, apart from using the most accurate velocity maps of Gaia DR3, we carry out a careful analysis of the many parts of the Jeans equations in the vertical direction. In particular, we realize how important it is to introduce a flare in the disk, especially at the largest  $R$ , or the inclusion of a double thin+thick disk rather than a single disk, the dependence of the scale height on the average age of the population, or more importantly, the stellar density distribution near the plane. An accurate measurement of the vertical velocity dispersion as a function of  $R, z$  is also important, and different selection effects, statistical methods, or fitting laws may vary the numbers (see Sects. 3.1, 3.4). In the end, we cannot have infinitely precise data to carry out our calculation, but we carry out a careful analysis of the effect of the most important sources of error bars.

A key question among the mentioned ones is whether the vertical distribution of stellar density follows an exponential law or  $\text{sech}^2$  law. Different observational

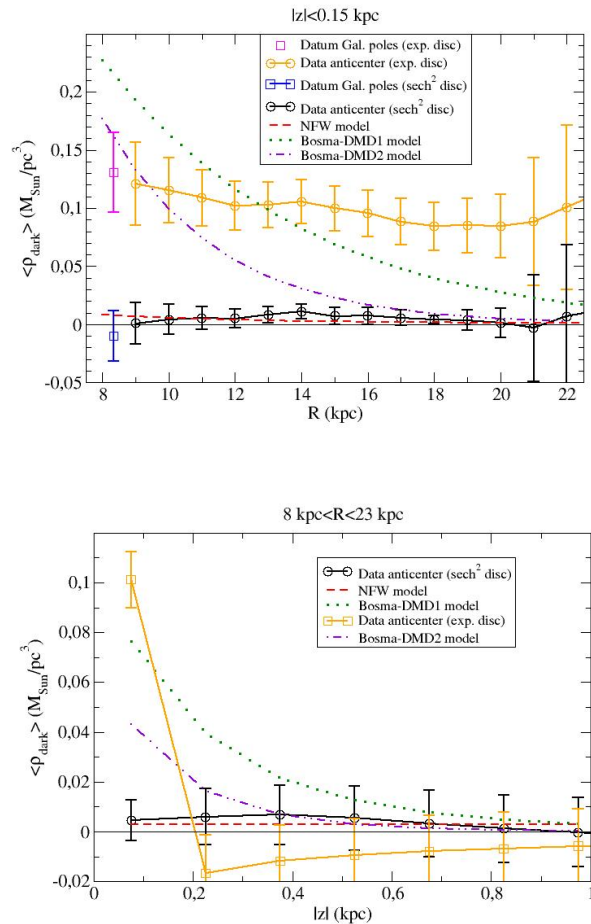


**Figure 15.** Average dark matter density derived from Eq. (25) assuming either exponential or  $\text{sech}^2$  (default) stellar vertical disk. Error bars include both the errors of the data and the errors in the visible matter model. Top: average within  $|z| < 0.15$  kpc, as a function of  $R$ . Bottom: average within  $8 \text{ kpc} \leq R \leq 23 \text{ kpc}$ , as a function of  $|z|$  within  $|z| < 1.05$  kpc in the anticenter region. Comparison with theoretical models.

works (e.g., Dobbie & Warren 2020; Everall et al. 2022; Chrobáková et al. 2022; Vieira et al. 2023) prefer one or the other solution. However, from a theoretical point of view, there is no possibility to choose among both: only one of them is consistent with the Jeans equations for a steady equilibrium disk, a  $\text{sech}^2$ , whereas the vertical exponential leads to the inconsistent result of  $\Sigma(R, z=0) \neq 0$ . With this in mind, we have used  $\text{sech}^2$  distributions for the visible (stars and gas+dust) matter, though in a few examples, we have checked the possible effects of changing to an exponential distribution, too.

Perhaps the most important result of the obtained surface density,  $\Sigma(R, z)$ , is that its error bars are quite large if one takes into account all of the factors that contribute to the Jeans equations and the modeling of the visible/baryonic matter. However, even with large error bars, we are able to set some modest constraints in the distribution of dark matter (within Newtonian gravity) or the compatibility of MOND. The results of our analyses can be summarized as follows: (i) the model of

the spherical dark matter halos in the NFW and MOND models are compatible with these data, though our data are not precise enough to corroborate the exact shape of  $\rho_{\text{dark}}$ ; (ii) the model of the disky dark matter with density proportional to the gas density (Bosma model) is totally excluded by the data; iii) the total lack of dark matter (there is only visible matter) within Newtonian gravity, is not very far from the data: only a  $2.6\sigma$  departure at  $R = 14$  kpc,  $|z| < 1.05$  kpc; taking into account that we have analyzed hundreds of bins of  $R$  and  $z$ , the probability of finding one with a departure of  $2.6\sigma$  is likely.

1. The first point is not a surprise and is in line with the results previously obtained by other researchers. Nevertheless, we would like to remark that compatibility does not mean confirmation of a model. Further research is necessary to be able to confirm the existence of these dark matter halos or modified gravity scenarios.
2. The second point is not a surprise either, although it serves to remind us of a serious obstacle in the development of a hypothesis that explains the rotation curve of spiral galaxies in terms of dark matter distributed in a disk rather than in a halo (Bosma 1981; Pfenninger et al. 1994; Feng & Gallo 2015; McKee et al. 2015; Fernández-Torija 2016; Kramer & Randall 2016; Sipols & Pavlovich 2021; Sylos Labini et al. 2023; 2024; Sylos Labini 2024). Indeed, it has been well known for many decades (Kuzmin 1952; 1955) that there is no evidence for the presence of dark matter in the disk of the Galaxy (from observations in the solar neighborhood). What we get here is that a disky dark matter predicts a dark matter density in in-plane regions ( $|z| < 0.15$  kpc) much higher than observed: we get  $\langle \rho_{\text{dark}} \rangle(R, |z| < 0.15) \lesssim 0.01 M_{\odot}/\text{pc}^3 \forall R$  between 8 and 12 kpc (see Fig. 8, top-left panel), whereas the disky dark matter between 0.05 and  $0.2 M_{\odot}/\text{pc}^3$  within that range of  $R$  is compatible with the rotation curves. The only way to save the model of disky dark matter is decoupling from gas density and allowing a much larger scale height [we would require a scale height at  $R < 12$  kpc to be larger than 600 pc ( $2\sigma$ ), which makes it closer to a spheroidal distribution, or substituting the  $\text{sech}^2$  stellar density for an exponential profile, which may solve the problem in in-plane regions but however is still inconsistent at larger  $|z|$  values.

Sylos Labini (2024) presents an opposite conclusion about the disky dark matter, using the same data. He claims that a DMD2 model fits the data with  $h_z \approx 100$  pc, of the order of the gas scale height, so it is compatible with Bosma hypothesis. However, this analysis by Sylos Labini (2024) has a series of oversimplifications and wrong assumptions that make his result invalid:

- (a) The hypothesis that the velocity distribution of dark matter particles and stars is the same one (Sylos Labini 2024, Eq. (12)) is not appropriate since the particles of a putative non-

baryonic dark matter would have different origins and formations.

- (b) The use of Equations (21) and (22) of Sylos Labini (2024) to calculate the average scale height includes dark matter and gas density distributions, which is not correct; the scale height should be that of the population of stars that are used to measure the dispersion of velocities (the stars), as stated in the Jeans equations (see the paragraph after Eq. (4) in this paper).
  - (c) There is a factor 2 in the Equations (28), (30), and (32) Sylos Labini (2024) that is not correct.
  - (d) Sylos Labini uses a mass of the thick disk equal to 90% of the mass of the thin disk, which is too high because the dominant disk should be the thin one; also, a scale length of 4.5 kpc for the thin disk is doubtful when using optical sources of Gaia (different from the scale length with near infrared surveys).
  - (e) The total  $\Sigma$  [(Sylos Labini 2024, Fig. 11/top panel); note that  $a_z = 2\pi G\Sigma$ ] cannot be used to fit and test the DMD2 model because  $\Sigma$  is dominated by the visible matter, and we need to subtract the visible matter separately to analyze the residuals of dark matter, as carried out here in Section 4.
  - (f) The fit of  $h_z(R)$  for DMD2 model given in Sylos Labini (2024, Fig. 11/bottom panel) avoids the points with  $|z| < 0.5$  kpc, which are precisely the ones giving the major discrepancy of a low  $h_z$  in DMD2 (see Fig. 5, bottom-left panel in this paper).
  - (g) The use of exponential vertical distribution instead of  $\text{sech}^2$  presents some differences in the regime  $|z| < 0.5$  kpc (see Fig. 15 of this paper). This might be a reason to avoid this range, but in any case, this range is necessary if we want to analyze a DMD2 model with most of its mass within it. DMD2 gives a local dark matter density in the solar neighborhood equal to  $\rho_{DMD2,\odot} = 0.18 M_{\odot}/\text{pc}^3$ , which is totally at odds with any other estimation, either in the present work or in many other analyses (none of the numbers allows a dark matter density larger than  $\sim 0.02 M_{\odot}/\text{pc}^3$ ; see references at point of 1 of Section 4.3).
3. The third point is remarkable, too. We see that the observed values of  $\Sigma$  derived from the dispersion of velocities are consistent with a mass distribution only with visible matter and Newtonian gravity. Previous analyses presented overwhelming evidence for a significantly nonzero value of  $\rho_{\text{dark}}(R_{\odot}, z = 0) = 0.01 - 0.02 M_{\odot}/\text{pc}^3$  (e.g., Garbari et al. 2012; Catena & Ullio 2012; Pato et al. 2015; Xia et al. 2016; de Salas & Widmark 2021; Ou et al. 2024), and  $\Sigma(R = R_{\odot}, z = 1 - 1.1\text{kpc}) = 50 - 80 M_{\odot}/\text{pc}^2$  (Horta et al. 2024, Table 1)(Nitschai et al. 2021), larger than the visible matter surface density and implying the necessity of dark matter.

However, we have seen in this paper how sensitive the derivations of  $\rho_{\text{dark}}$  are based on kinematic data on the different assumptions modeling the stellar density distribution, and dark matter can only be detected through the kinematical effects. We obtained  $\Sigma(R = R_{\odot}, z = 0.9 \text{ kpc}) = 43 \pm 11 \text{ M}_{\odot} \text{ pc}^{-2}$ ,  $\Sigma(R = R_{\odot}, z = 1.05 \text{ kpc}) = 39 \pm 18 \text{ M}_{\odot} \text{ pc}^{-2}$  (within Newtonian gravity), lower than the most common values in the literature and compatible with expected surface density for visible matter alone [ $\Sigma_{\text{vis.}}(R = R_{\odot}, z = 0.9 \text{ kpc}) = 42.8 \text{ M}_{\odot} \text{ pc}^{-2}$ ;  $\Sigma_{\text{vis.}}(R = R_{\odot}, z = 1.05 \text{ kpc}) = 43.7 \text{ M}_{\odot} \text{ pc}^{-2}$  from Fig. 7], thus allowing zero dark matter. These larger error bars are not due to worse data or a more awkward technique, but to a more strict modeling of the stellar distribution (see Sect. 3.9). We agree with Cheng et al. (2024) that the measured mass density is highly dependent on the assumptions when using the Jeans equations. In general, the analysis of the Jeans equations is (stellar density) model dependent, and a 3% relative error in  $\Sigma(R = R_{\odot}, z = 1.1 \text{ kpc})$ , as given in Nitschai et al. (2021) looks too optimistic, given that the uncertainties in the scale height and  $\sigma_{V_z}$  are much larger than this.

In other words, we cannot reject the hypothesis of a dark matter halo (with very low density near the plane), but we cannot prove it either. Given that the proof of the existence of (non-baryonic) dark matter on Galactic scales is still being discussed, and there are many inconsistencies and tensions pending to be solved (López-Corredoira 2022, §3.4), and with rotation curves in the Milky Way allowing a large range of solutions even without dark matter (MOND or also within Newtonian gravity), our results make us think that the hypothesis of the existence of dark matter halos is less solid than we thought. Therefore, still, even in the epoch of accurate measurements of stellar velocities with *Gaia* data, we must take the hypothesis of the existence of dark matter with a grain of salt, which is more supported by cosmological speculations than by the observations of galaxies.

We thank the referee for a thorough and very helpful review and detailed comments, which improved the quality of the paper. Thanks are given to Francesco Sylos Labini for valuable comments, and the fittings in Section 3.3 and Figure 3. Thanks are given to Juan Betancort-Rijo and Roberto Capuzzo-Dolcetta for discussions on the applicability of the Jeans equations. This research was supported by the Chinese Academy of Sciences President's International Fellowship Initiative grant No. 2023VMB0001 and grant No. PID2021-129031NB-I00 from the Spanish Ministry of Science (MICINN). This work has made use of data from the European Space Agency (ESA) mission *Gaia* (<https://www.cosmos.esa.int/gaia>), processed by the *Gaia* Data Processing and Analysis Consortium (DPAC), <https://www.cosmos.esa.int/web/gaia/dpac/consortium>). Funding for the DPAC has been provided by national

institutions, in particular, the institutions participating in the *Gaia* Multilateral Agreement.

## ORCID FOR AUTHORS

M. López-Corredoira: 0000-0001-6128-6274

## REFERENCES

- Amôres, E. B., Robin, A. C., Reylé, C. 2017, *A&A*, 602, A67  
 Battinelli, P., Demers, S., Rossi, C., & Gigoyan, K. S. 2013, *Astrophysics*, 56, 68  
 Bekenstein, J., & Milgrom, M. 1984, *ApJ*, 286, 7  
 Bilir, S., Cabrera-Lavers, A., Karaali, S., Ak, S., Yaz, E., & López-Corredoira, M. 2008, *PASA*, 25, 69  
 Binney, J., & Tremaine, S. 2008, *Galactic Dynamics*, 2nd. ed., Princeton Univ. Press, Princeton  
 Bosma, A. 1981, *AJ*, 86, 1791  
 Bovi, J., & Tremaine, S. 2012, *ApJ*, 756, 89  
 Brand, J., & Blitz, L. 1993, *A&A*, 275, 67  
 Callingham, T. M., Cautun, M., Deason, A. J., et al. 2019, *MNRAS*, 484, 5453  
 Candlish, G. N., Smith, R., Moni Bidin, C., & Gibson, B. K. 2016, *MNRAS*, 456, 3456  
 Catena, R., & Ullio, P. 2012, *JCAP*, 5, 005  
 Chan, M. H., & Law, K. C. 2023, *ApJ* 957, 24  
 Cheng, X., Anguiano, B., Majewski, S. R., & Arras, P. 2024, *MNRAS*, 527, 959  
 Chrobáková, Z., & López-Corredoira, M. 2021, *ApJ*, 912, 130  
 Chrobáková, Z., López-Corredoira, M., Sylos Labini, F., Wang, H.-F., & Nagy, R. 2020, *A&A*, 642, A95  
 Chrobáková, Z., Nagy, R., & López-Corredoira, M. 2022, *A&A*, 664, A58  
 Ciotti, L. 2021, *Introduction to Stellar Dynamics*, Cambridge Univ. Press, Cambridge  
 Clemens, D. P. 1985, *ApJ*, 295, 422  
 de Salas, P. F., & Widmark, A. 2021, *Rep. Prog. Phys.*, 84, 104901  
 Dobbie, P. S., & Warren, S. J. 2020, *Open J. Astrophys.*, 3, 5  
 Drimmel, R., Romero-Gómez, R., Chemin, L., et al. 2023, *A&A*, 674, A37  
 Eilers, A.-C., Hogg, D. W., Rix, H.-W. & Ness, M. K. 2019, *ApJ*, 871, 120  
 Everall, A., Evans, N. W., Belokurov, V., Boubert, D., & Grand, R. J. J. 2022, *MNRAS*, 511, 2390  
 Famaey, B., & McGaugh, S. 2012, *Living Rev. Relativity*, 15, 10  
 Feng, J. Q., & Gallo, C. F. 2015, *Phys. Int.*, 6, 11  
 Fernández-Torija Daza, G. 2016, *Relationship between rotation curves and matter distribution in spiral galaxy discs*, Master Thesis, Univ. La Laguna (Spain) [arXiv:2003.4951]  
 Finzi, A. 1963, *MNRAS* 127, 21  
 Gaia Collaboration 2018, *A&A*, 616, A11  
 Gaia Collaboration 2023, *A&A*, 674, A1  
 Galazutdinov, G., Strobel, A., Musaeov, F. A., Bondar, A., & Krelowski, J. 2015, *PASP*, 127, 126  
 Garbari, S., Liu, C., Read, J. I., & Lake, G. 2012, *MNRAS*, 425, 1445  
 Guo, R., Li, Z.-Y., Shen, J., Mao, S., & Liu, C. 2024, *ApJ*, 960, 133  
 Hessman, F. V. 2015, *A&A*, 579, A123  
 Honma, M., & Sofue Y. 1996, *PASJ* 48, L103  
 Honma, M., Nagayama, T., Ando, K., et al. 2012, *PASJ*, 64, 136  
 Horta, D., Price-Whelan, A. M., Hogg, D. W., Johnston, K. V., Widrow, L., Dalcanton, J. J., Ness, M. K., & Hunt, J. A. S. 2024, *ApJ*, 962, 165  
 Jiao, Y., Hammer, F., Wang, H., Wang, J., Amram, P., Chemin, L., & Yang, Y. 2023, *A&A*, 678, A208  
 Kalberla, P. M. W., & Dedes, L. 2008, *A&A*, 487, 951  
 Katz, D., Sartoretti, P., Guerrier, A., et al. 2023, *A&A*, 674, A5  
 Koop, O., Antoja, T., Helmi, A., Callingham, T. M., & Laporte, C. F. P. 2024, *A&A* 692, A50  
 Kramer, E. D., & Randall, L. 2016, *ApJ*, 829, 126  
 Kuzmin, G. G. 1952, *Tartu Astr. Obs. Publ.* 32, 5  
 Kuzmin, G. G. 1955, *Tartu Astr. Obs. Publ.* 33, 3  
 Li, C., Zhao, G., Jia, Y., Liao, S., Yang, C., & Wang, Q. 2019, *ApJ*, 871, 208

- Loebman, S. R., Ivezić, Z., Quinn, T. R., Governato, F., Brooks, A. M., Christensen, C. R., & Jurić, M. 2012, *ApJL*, 758, L23
- López-Corredoira, M. 2022, *Fundamental Ideas in Cosmology. Scientific, philosophical and sociological critical perspective*, IoP-Science, Bristol
- López-Corredoira, M., Beckman, J. E., & Casuso, E. 1999, *A&A*, 351, 920
- López-Corredoira, M., & Betancort-Rijo, J. 2021, *ApJ*, 909, 137
- López-Corredoira, M., Betancort-Rijo, J., & Beckman, J. E. 2002a, *A&A*, 386, 169
- López-Corredoira, M., Cabrera-Lavers, A., Garzón, F., & Hammersley, P. L. 2002b, *A&A*, 394, 883
- López-Corredoira, M., Garzón, F., Wang, H.-F., Sylos Labini, F., Nagy, R., Chrobáková, Z., Chang, J., & Villarroel, B. 2020, *A&A*, 634, A66
- López-Corredoira, M., & Sylos Labini, F. 2019, *A&A*, 621, A48
- McKee, C. F., Parravano, A., & Hollenbach, D. J. 2015, *ApJ*, 814, 13
- MacKereth, J. T., Bovy, J., Schiavon, R. P., et al. 2017, *MNRAS*, 471, 3057
- Moni Bidin, C., Carraro, G., & Méndez, R. A. 2012a, *ApJ*, 747, 101
- Moni Bidin, C., Carraro, G., Méndez, R. A., & Smith, R. 2012b, *ApJ*, 751, 30
- Moni Bidin, C., Smith, R., Carraro, G., Méndez, R. A., & Moyano, M. 2015, *A&A*, 573, A91
- Nitschai, M. S., Eilers, A.-C., Neumayer, N., Cappellari, M., & Rix, H.-W. 2021, *ApJ*, 916, 112
- Olling, R. P., & Merrifield, M. R. 2000, *MNRAS*, 311, 361
- Ou, X. W., Eilers, A. C., Necib, L., & Frebel, A. 2024, *MNRAS*, 528, 693
- Pato, M., Iocco, F., & Bertone, G. 2015, *JCAP*, 12, 001
- Pfenniger, D., Combes, F., & Martinet, L. 1994, *A&A*, 285, 79
- Poggio, E., Drimmel, R., Andrae, R., et al. 2020, *Nat. Astron.*, 4, 590
- Pont, F., Queloz, D., Bratschi, P., & Mayor, M. 1997, *A&A*, 318, 416
- Rana, N. C., & Basu, S. 1992, *A&A*, 265, 499
- Reid, R. J., Menten, K. M., Brunthaler, A., et al. 2014, *ApJ*, 783, 130
- Robin, A. V., Reylé, C., Derrière, S., & Picaud, S. 2003, *A&A*, 409, 523
- Sakamoto T., Chiba M., & Beers T. C. 2003, *A&A* 397, 899
- Sanders, J. 2012, *MNRAS*, 425, 2228
- Sanders, R. H., & McGaugh, S. S. 2002, *ARA&A*, 40, 263
- Sánchez-Salcedo, F. J., Flynn, C., & de Diego, J. A. 2016, *ApJ*, 817, 13
- Sipols, A., & Pavlovich, A. 2021, *Galaxies*, 8, 36
- Sofue, Y. 2009, *PASJ*, 61, 153
- Sofue, Y. 2015, *PASJ*, 67, 75
- Sofue, Y., Honma, M., & Omodaka, T. 2009, *PASJ*, 61, 227
- Sylos Labini, F. 2024, *ApJ*, 976, 185
- Sylos Labini, F., Chrobáková, Z., Capuzzo-Dolcetta, R., & López-Corredoira, M. 2023, *ApJ*, 945, 3
- Sylos Labini, F., De Marzo, G., Straccamore, M., & Comerón, S. 2024, *MNRAS*, 527, 2697
- Toomre, A. 1981, in: D. M. Fall & D. Lynden-Bell, eds, ‘The Structure and Evolution of Normal Galaxies’, Cambridge University Press, Cambridge (U.K.), pp. 111–136.
- Vieira, K., Korchagin, V., Carraro, G., & Lutsenko, A. 2023, *Galaxies*, 11, 77
- Villa Durango, M. A. 2022, *Dinámica y distribución en el disco grueso de la Galaxia*, Master Thesis, Univ. de Antioquia (Colombia)
- Wang, H.-F., Chrobáková, Z., López-Corredoira, M., & Sylos Labini, F. 2023, *ApJ*, 942, 12
- Xia, Q., Liu, C., Mao, S., et al. 2016, *MNRAS* 458, 3859
- Zhu, Y., Ma, H.-X., Dong, X.-B., et al. 2023, *MNRAS*, 519, 4479

## APPENDIX

## JEANS EQUATIONS FOR A MULTICOMPONENT DISTRIBUTION

Given a single stellar population component  $i$  with a given density  $\rho_i = \frac{N_i}{\mathcal{V}}$  ( $\mathcal{V}$  is volume of each bin;  $N_i$  its number of stars), average velocity distribution  $V_{z,i}$ , the Jeans equations for the vertical direction (the reasoning would be similar for the radial direction), applying Eq. (4), neglecting the terms with  $V_R V_z$  (see Sect. 3.4), is

$$a_z(R, z) = -\frac{1}{N_i(R, z)} \frac{\partial [N_i(R, z) V_{z,i}^2(R, z)]}{\partial z} \quad (\text{A1})$$

On average for all components,

$$\bar{\rho} = \frac{\sum_i N_i}{\mathcal{V}}, \quad (\text{A2})$$

$$\overline{V_z^2} = \frac{\sum_i N_i V_{z,i}^2}{\sum_i N_i} \quad (\text{A3})$$

$$\overline{\rho V_z^2} = \frac{\sum_i N_i V_{z,i}^2}{\mathcal{V}} = \bar{\rho} \overline{V_z^2} \quad (\text{A4})$$

Hence, using Eq. (A1),

$$\frac{\partial [\overline{\rho V_z^2}(R, z)]}{\partial z} = -\frac{a_z(R, z)}{\mathcal{V}} \sum_i N_i(R, z) = -a_z(R, z) \bar{\rho}. \quad (\text{A5})$$

Reordering the terms, we have the Jeans equations for the multicomponent system:

$$a_z(R, z) = -\frac{1}{\bar{\rho}} \frac{\partial [\overline{\rho V_z^2}(R, z)]}{\partial z}. \quad (\text{A6})$$

CALCULATION OF  $\sigma_{V_z}$  FOR A DISTRIBUTION WITHOUT HIGH-VELOCITY STARS

In a distribution of velocities assumed to be Gaussian but without the tails of high-velocity stars ( $|V_z| > V_c$ ), the calculation of  $\sigma_{V_z}$  is

$$\sigma_{V_z} = \sqrt{\sigma_{V_z}^2 \operatorname{erf}\left(\frac{V_c}{\sqrt{2}\sigma_{V_z}}\right) + \frac{2}{\sqrt{2\pi}\sigma_{V_z}} \left[ \int_{V_c}^{\infty} dx x^2 \exp\left(-\frac{x^2}{2\sigma_{V_z}^2}\right) \right]}, \quad (\text{B1})$$

which is solved iteratively for  $\sigma_{V_z}$ , with the first iteration equal to

$$\sigma_{V_z,0} = \sqrt{\langle V_z^2 \rangle - \langle V_z \rangle^2}. \quad (\text{B2})$$

For our practical case of  $V_c = 100$  km/s,  $V_c$  is 2.5-5 times  $\sigma_{V_z,0}$ , so this correction is very small, and  $\sigma_{V_z}$  is very close to  $\sigma_{V_z,0}$ . We could even neglect this correction. In any case, the above equation is exact for any cutoff of the Gaussian tail, and the calculation of  $\sigma_{V_z}$  would not be affected if we set a tighter constraint in the selection of non-high-velocity stars.